HHS Public Access

Author manuscript

Cell Rep. Author manuscript; available in PMC 2019 December 30.

Published in final edited form as:

Cell Rep. 2019 December 03; 29(10): 3060–3072.e7. doi:10.1016/j.celrep.2019.10.071.

Overcoming Steric Restrictions of VRC01 HIV-1 Neutralizing Antibodies through Immunization

K. Rachael Parks[1,2], **Anna J. MacCamy**[1], **Josephine Trichka**[1], **Matthew Gray**[1], **Connor Weidle**[1], **Andrew J. Borst**[3], **Arineh Khechaduri**[1], **Brittany Takushi**[1], **Parul Agrawal**[1], **Javier Guenaga**[4], **Richard T. Wyatt**[4], **Rhea Coler**[2,5], **Michael Seaman**[6], **Celia LaBranche**[7], **David C. Montefiori**[7], **David Veesler**[3], **Marie Pancera**[1,8,*], **Andrew McGuire**[1,2,*], **Leonidas Stamatatos**[1,2,9,*]

[1]Vaccines and Infectious Diseases Division, Fred Hutchinson Cancer Research Center, Seattle, WA, USA

[2]Department of Global Health, University of Washington, Seattle, WA, USA

[3]Department of Biochemistry, University of Washington, Seattle, WA, USA

[4]IAVI Neutralizing Antibody Center, Department of Immunology and Microbiology, The Scripps Research Institute, San Diego, CA, USA

[5]Infectious Disease Research Institute, Seattle, WA, USA

[6]Beth Israel Deaconess Medical Center, Harvard Medical School, Boston, MA, USA

[7]Laboratory for AIDS Vaccine Research and Development, Duke University, Durham, NC, USA

[8]Vaccine Research Center, National Institutes of Allergy and Infectious Diseases, NIH, Bethesda, MD, USA

[9]Lead Contact

SUMMARY

Broadly HIV-1 neutralizing VRC01 class antibodies target the CD4-binding site of Env. They are derived from VH1–2*02 antibody heavy chains paired with rare light chains expressing 5-amino acid-long CDRL3s. They have been isolated from infected subjects but have not yet been elicited by immunization. Env-derived immunogens capable of binding the germline forms of VRC01 B cell receptors on naive B cells have been designed and evaluated in knockin mice. However, the

*Correspondence: mpancera@fredhutch.org (M.P.), amcguire@fredhutch.org (A.M.), lstamata@fredhutch.org (L.S.).

AUTHOR CONTRIBUTIONS

Conceptualization, K.R.P., A.M., and L.S.; Methodology, K.R.P., C.W., A.J.B., D.V., M.P., and L.S.; Investigation, K.R.P., A.J.M., J.T., M.G., C.W., A.J.B., A.K., B.T., P.A., J.G., R.T.W., R.C., C.L., and D.C.M.; Visualization, K.R.P., A.J.M., J.T., C.L., C.W., A.J.B., and M.P.; Writing – Original Draft, K.R.P. and L.S.; Writing – Review & Editing, all authors; Funding Acquisition, L.S., D.C.M., and D.V.; Supervision, M.P. and L.S.

DECLARATION OF INTERESTS

The authors declare no competing interests. Patent US 2018/0117140 “Engineered and Multimerized Human Immunodeficiency Virus Envelope Glycoproteins and Uses Thereof” was awarded to A.M. and L.S.

SUPPLEMENTAL INFORMATION

Supplemental Information can be found online at https://doi.org/10.1016/j.celrep.2019.10.071.

elicited antibodies cannot bypass glycans present on the conserved position N276 of Env, which restricts access to the CD4-binding site. Efforts to guide the appropriate maturation of these antibodies by sequential immunization have not yet been successful. Here, we report on a two-step immunization scheme that leads to the maturation of VRC01-like antibodies capable of accommodating the N276 glycan and displaying autologous tier 2 neutralizing activities. Our results are relevant to clinical trials aiming to elicit VRC01 antibodies.

In Brief

The conserved N276 glycan on the HIV-1 Env presents a major steric hindrance in the maturation of VRC01-class bnAbs. Here, Parks et al. discuss a two-step immunization scheme that leads to the development of VRC01-like antibodies that accommodate the N276 glycan on heterologous Env-derived proteins yet display limited neutralizing activities.

Graphical Abstract

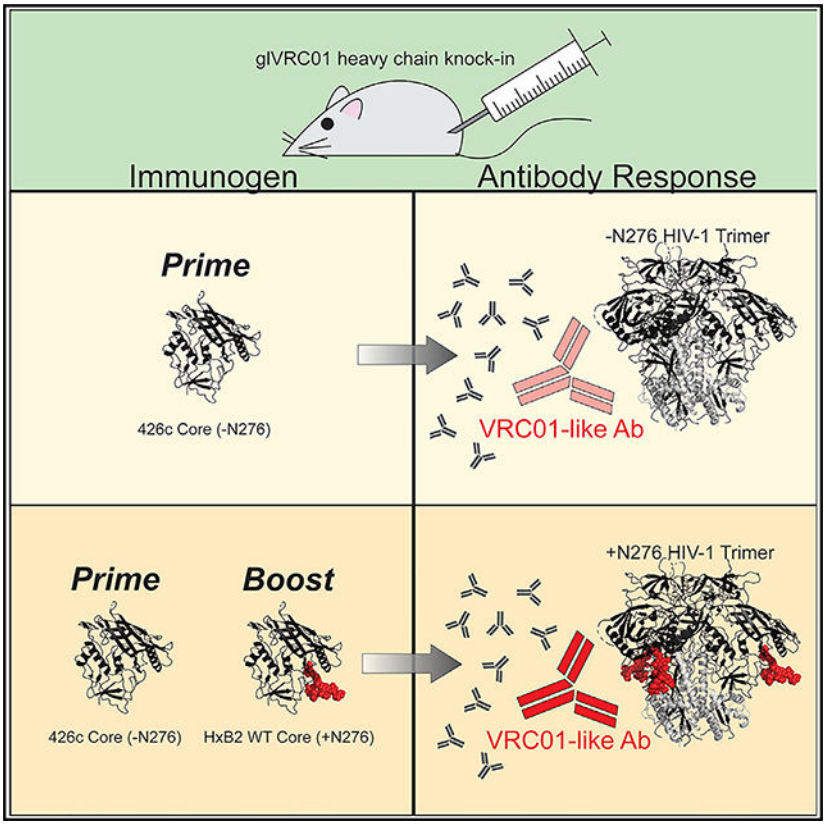

INTRODUCTION

VRC01-class antibodies are potent and broad HIV-1 neutralizing antibodies (bnAbs) that offer protection from experimental animal (S)HIV (simian HIV) infection (Balazs et al., 2014; Gautam et al., 2016; Pegu et al., 2014; Shingai et al., 2014), and could be an important component of the protective immune responses elicited by an effective HIV-1 vaccine (Burton and Hangartner, 2016; Kwong and Mascola, 2018). They have been isolated from

several HIV-1-infected subjects and share key genetic origins: their heavy chain (HC) V genes are derived from the VH1–2*02 allele and are paired with light chains (LCs) expressing 5-amino acid (aa)-long CDRL3, which is rarely found in the human antibody repertoire. The 5-aa CDRL3 contains a hydrophobic residue at position 91 and a Glu96 (Scheid et al., 2011; Wu et al., 2010, 2011; Zhou et al., 2013, 2015). The VRC01-class bnAbs are extensively somatically hypermutated (up to 30% aa difference from germline) and can be up to 50% divergent in aa sequence (Scheid et al., 2011; Wu et al., 2010, 2011; Zhou et al., 2010, 2015). Despite this marked diversity, their CDR domains adopt similar overall structures and recognize the CD4-binding site (CD4-BS) of Env in a manner similar to that of CD4 (Zhou et al., 2010, 2013). Thus, despite their similar genetic origins, during chronic infection with different HIV-1 viruses, VRC01-class antibodies mature along different pathways but ultimately adopt similar structures that are associated with their broad neutralizing activity. The “structural convergent evolution” observed during natural HIV-1 infection suggests that more than one evolutionary pathway will be available to develop VRC01-class bnAbs by immunization.

Longitudinal natural viral Env variants associated with the development of bnAbs against the Env apex region (Doria-Rose et al., 2014) and of non-VRC01-class anti-CD4-BS bnAbs have been identified and characterized (Bonsignori et al., 2016; Liao et al., 2013). Viral Envs associated with the maturation of VRC01-class antibody responses have also been reported in the case of chronic HIV-1 infection (Bonsignori et al., 2018; Lynch et al., 2015), but such viral Envs were derived from samples collected after the VRC01 B cells lineages had already expanded. More recently however, Umotoy et al. (2019) reported on the longitudinal evolution of virus and VRC01-class B cell lineages in an HIV-1-infected patient from protocol C. So far, however, the natural Env(s) that initiated the production of VRC01-class antibodies during HIV-1 infection have yet to be identified. Also, the inferred germline forms of VRC01-class antibodies (commonly referred to as glVRC01 Abs), do not display detectable reactivity to diverse recombinant Env-derived soluble proteins (Hoot et al., 2013; Jardine et al., 2013; McGuire et al., 2013). In recent years, we and others reported on the design of “germline VRC01-targeting” recombinant Env-derived proteins capable of binding glVRC01-class Abs (Jardine et al., 2013, 2015; McGuire et al., 2013, 2014, 2016; Medina-Ramírez et al., 2017). A key feature of such immunogens is the absence of the conserved N-linked glycosylation site (NLGS) at position 276 within loop D of the gp120 Env subunit, as the N276-associated glycans present a major barrier to glVRC01 Ab binding, through steric obstruction of the germline-encoded CDRL1s (Borst et al., 2018; McGuire et al., 2013; Zhou et al., 2013). Mature VRC01 bnAbs accommodate this glycan by either incorporating glycine residues in their CDRL1 domains or by shortening them during affinity maturation (Zhou et al., 2013).

Although VRC01 germline-targeting immunogens activate B cells engineered to express glVRC01-class B cell receptors (BCRs) *in vitro* and *in vivo* (Jardine et al., 2013, 2015; McGuire et al., 2013, 2014, 2016; Medina-Ramírez et al., 2017), these cells undergo limited somatic mutation and the secreted antibodies fail to bind in the presence of N276-associated glycans on wild-type (WT) Envs (Dosenovic et al., 2015; Jardine et al., 2015; McGuire et al., 2016). Efforts to guide the maturation of VRC01-like antibody responses elicited by germline-targeting immunogens through subsequent immunizations with heterologous Env-

derived proteins also lacking the N276 glycans, led to increased somatic mutations, in both the VH and VL antibody genes, but no direct evidence that the elicited antibodies could accommodate N276-associated glycans was provided (Briney et al., 2016; Tian et al., 2016).

Here, we report on a two-step immunization scheme that begins with a prime immunization with the VRC01 germline-targeting prime immunogen, 426c Core, that lacks the N276 NLGS, followed by a boost immunization with a heterologous Env-derived immunogen, harboring the 276 NLGS. The outcome of this immunization scheme was the production of VRC01-like antibodies capable of accommodating the steric block imposed by the glycans present at N276 on heterologous gp120 Core-derived Envs and neutralizing the autologous, tier 2 426c virus with a modified glycan shield.

RESULTS

The 426c Core Germline-Targeting Immunogen Elicits Potent Plasma Antibody Responses against the VRC01 Epitope in Knockin Mice

We previously reported on the design of a recombinant protein derived from the inner and outer gp120 domains of the clade C Env 426c, lacking the variable domains 1, 2, and 3 as well as three NLGS at positions N276 (loop D), N460, and N463 (V5). That protein (TM4ΔV1–3, herein referred to as “426c Core” for simplicity) binds several of the known glVRC01-class Abs (McGuire et al., 2016). Here, two nanoparticle forms of the 426c Core were employed as immunogens: a 5- to 7-meric form (426c Core C4b) (Hofmeyer et al., 2013; McGuire et al., 2016; Ogun et al., 2008) and a Ferritin-based 24-meric form (426c Core Fer) (Kanekiyo et al., 2013; McGuire et al., 2016). One additional germline VRC01-targeting immunogen was investigated for its ability to engage B cells expressing glVRC01 BCRs *in vivo*: the 426c DS-SOSIP D3 (Borst et al., 2018; Joyce et al., 2017). It is derived from the clade C 426c virus (like the 426c Core) and was modified by eliminating the above-mentioned three NLGSs. We also performed an immunization with the non-germline targeting unmodified 426c WT gp120 as a control.

As animal species, such as mice, rats, rabbits, or non-human primates do not express orthologs of the human VH1–2*02 allele (Jardine et al., 2013; Vigdorovich et al., 2016; West et al., 2012), immunizations were performed in a knockin mouse that is heterozygous for the glVRC01 HC, whereas the LCs remain the endogenous mouse LCs (mLCs) (Jardine et al., 2015). Approximately 80% of naive B cells express the glVRC01 HC and 0.1% of mLCs express 5-aa-long CDRL3s. Thus, the overall estimated frequency of naive B cells expressing potential glVRC01 BCRs in this mouse model is approximately 0.08% (compared to approximately 0.01% in humans; Arnaout et al., 2011; DeKosky et al., 2015; Jardine et al., 2015). The elicitation of VRC01-class bnAbs in this model requires overcoming at least two major obstacles: first, the germline-targeting immunogen must select for the B cells expressing extremely rare mLCs with a 5-aa CDRL3 paired with the glVRC01 HC, and second, the immunization regimen must lead to the accumulation of mutations that will allow the maturing B cells to bypass the obstacles presented by the N276 glycans on full-length Envs.

A single immunization with either nanoparticle form of 426c Core with two different adjuvants (poly(I:C) or GLA-LSQ) elicits robust autologous plasma antibody responses (Figure 1A), the majority of which target the CD4-BS (Figure 1B). Plasma antibodies generated in approximately 77% of the 426c Core-immunized animals (66 of 85), also recognized the heterologous VRC01 germline-targeting immunogen eOD-GT8 (Figure 1C) in a VRC01 epitope-dependent manner (Figures S1A and S1B). eOD-GT8 is derived from the outer domain of the gp120 subunit of the clade B HxB2 Env (Jardine et al., 2013, 2015). Thus, antibodies elicited by the 426c Core that recognize eOD-GT8, but not the eOD-GT8 knockout (KO) (not recognized by VRC01-class antibodies) are most likely VRC01 epitope-specific. In contrast, the 426c DS-SOSIP D3 germline-targeting immunogen elicited very weak autologous plasma antibody responses and only one animal elicited antibodies against the 426c Core, which were non-CD4-BS directed and did not recognize eOD-GT8 (Figure S1C). Animals immunized with the non-germline-targeting Env 426c WT gp120 immunogen elicited strong autologous responses, but weak anti-426c Core antibody responses and no eOD-GT8 antibody response (Figure S1D).

We concluded that the 426c Core immunogen elicits potent anti-CD4-BS antibody responses, which recognize the VRC01 epitope.

426c Core Selects for Key Mutations in the Antibody HC and LCs

To directly demonstrate that the 426c Core expands VRC01-lineage B cells, 2 weeks after immunization, eOD-GT8^{+}/eOD-GT8 KO^{-} specific class-switched B cells from the spleens and lymph nodes (LNs) of mice displaying plasma antibody cross-reactivity to eOD-GT8 were sorted and their VH/VL genes were sequenced. eOD-GT8^{+}/eOD-GT8 KO^{-} B cells were also sorted from unimmunized animals (a summary of the sequence analysis is presented in Figure S2). A total of 420 eOD-GT8+/eOD-GT8 KO^{-} class-switched B cells were singly sorted from the immunized animals and their VH and VL genes were amplified using PCR. 204 HC and 70 LCs were successfully sequenced (Figures S2A and S2C).

96% of HCs were VH1–2*02 (Figures 1D and S2B). In the majority (approximately 70%) of VH1–2*02 HCs isolated after the prime immunization, the histidine at position 35 in the CDRH1 domain was replaced by an asparagine (Figure S4A). The H35N mutation introduces an additional hydrogen bond with N100a in CDRH3 and increases the stability of interaction between CDRH1 and CDRH3 on VRC01-class antibodies (Jardine et al., 2015).

Approximately 57% of mLCs contained 5-aa-long CDRL3s (Figures 1E and S2E). The majority of the 5-aa CDRL3s are derived from the mouse 8–30*01 LC V gene, which is represented at approximately 6% in the naive eOD-GT8^{+}/eOD-GT8 KO^{-} B cell repertoire (Figures 1F and S2D). Other mLCs that utilized a 5-aa CDRL3 are derived from V-genes: 12–46*01, 4–61*01, 4–72*01, and 6–25*01 (representing 2.5% of the LC sequences with 5 aa each). All the identified 5-aa-long CDRL3s-containing mLCs were paired with glVRC01 HCs. Immunization with the 426c Core therefore preferentially expanded B cells expressing mLCs with 5-aa-long CDRL3s. A large fraction (40%) of the 5-aa-long CDRL3s contained a $Glu96_{LC}$ (Figures 1G and S2F), which is a key feature of mature VRC01-class antibodies and forms a hydrogen bond with $Gly459_{gp120}$ at the N terminus of the V5 region (West et

al., 2012; Zhou et al., 2013). In contrast, 5-aa-long CDRL3s with $Glu96_{LC}$ were not detected in the mLC sequenced from naive eOD-GT8^{+}/eOD-GT8 KO^{-} B cells (Figures 1G and S2F).

19 VH/VL pairs with VRC01 characteristics were expressed as IgGs (designated by "P" to indicate they were isolated following the prime immunization). All bound 426c Core and displayed no reactivity with 426c Core CD4-BS KO (Figure 1H). All 19 monoclonal antibodies (mAbs) also bound the eOD-GT8 protein, but not the eOD-GT8 KO (Figure 1I). As expected, the binding affinities of these antibodies for eOD-GT8 were higher than for 426c Core (Figure S3).

A 3.6-Å resolution crystal structure of antibody P-p3b3 bound to the 426c Core and a 3.2-Å resolution crystal structure of antibody P-p1f1 bound to eOD-GT8 were solved (Figure 2; Table S1). These antibodies bind 426c Core and eOD-GT8 with the same angles of approach that human glVRC01 binds 426c WT Core (all atoms root-mean-square deviation [RMSD] = 0.3 Å for gp120-Fv) (Borst et al., 2018) or eOD-GT6 (all atoms RMSD = 0.8 Å for gp120-Fv) (Jardine et al., 2013) (Figure 2A). Critical contacts, both in the HC (Figure 2B) and in the LC (Figure 2C), were maintained in these interactions: $Trp50_{HC}$, $Asn58_{HC}$, $Arg71_{HC}$, and $Trp100B_{HC}$ residues were not mutated in the mouse VRC01-like antibodies, adopted the same orientations, and participated in the same hydrogen bonding as observed with glVRC01 (Figure 2B). Similar to the human glVRC01 antibody, the short 5-aa CDRL3 of the mouse VRC01-like antibodies facilitates the interactions with gp120, and $Glu96_{LC}$ maintains the hydrogen bonds with Gly459 and Asn280 of gp120. Only a few residues in the LC seem to contact the gp120, and they are located at the N terminus, CDRL1 and CDRL3 (Figure 2C). The mouse VRC01-like antibodies have longer CDRL1 than most human VRC01-class antibodies (17 versus 11–12 aa long based on the Kabat nomenclature); however, several human VRC01-class antibodies, including VRC01c-HuGL2, have been isolated by sorting naive B cells with eOD-GT8 that contain 17-aa-long CDRL1 whose sequence is similar to that of the VRC01-like antibodies identified here (Figure 2C) (Havenar-Daughton et al., 2018; Jardine et al., 2016). Whereas the shorter CDRL1 domain of the human inferred glVRC01 Ab is well ordered in the complex of this antibody with eOD-GT6 (Jardine et al., 2013) or with 426c WT Core (Borst et al., 2018), the CDRL1 of the mouse VRC01-like antibodies bound to 426c Core or eOD-GT8 and that of VRC01c-HuGL2 bound to eOD-GT8 (Jardine et al., 2016) were disordered, indicating extensive CDRL1 flexibility. Such flexibility is likely necessary to accommodate glycans present on N276 in the presence of longer CDRL1. We concluded that the 426c Core immunogen elicits antibodies with similar genetic and structural features of known human VRC01-class antibodies.

Antibodies Elicited by the 426c Core Neutralize the 426c Virus Lacking the N276-Associated Glycans

Eight of the above 19 mAbs were tested for binding to stabilized soluble trimeric Envs (SOSIP or NFL). None bound the autologous 426c WT DS-SOSIP (Figure 3A); however, all bound to the derivative lacking the 276, 460, and 463 NLGS (426c DS-SOSIP D3) (Figure 3B), and seven bound the derivative only lacking the 276 NLGS (426c ΔN276 DS-SOSIP) (Figure 3C). Those seven mAbs also bound the heterologous 45_01dG5 NFL TD-2CC+(DS

+) trimer (Figure 3D). 45_01dG5 Env is derived from a virus that circulated in patient 45, from which several VRC01-class antibodies have been isolated (including VRC01), and naturally lacks the 276 and 460 NLGS (Lynch et al., 2015). mAb P-p1e7 did not bind to autologous or ΔN276 heterologous stabilized trimeric Envs and is the only antibody of those tested that lacks $Glu96_{LC}$ (Figure S4).

The neutralizing potency of four mAbs were evaluated against the WT 426c virus or its Δ276 NLGS derivative (Figure 3E) produced in either 293T or 293 $GnTI^{-/-}$ cells; viruses produced in 293 $GnTI^{-/-}$ cells can be used to detect the presence of glVRC01 class antibody neutralizing activities (Briney et al., 2016; LaBranche et al., 2018). In agreement with the binding data, the mAbs did not neutralize the WT 426c virus (regardless of whether it was produced in 293T or 293 $GnTI^{-/-}$ cells). However, three of four mAbs neutralized the $GnTI^{-/-}$ produced Δ276 NLGS virus, but not when produced in 293T cells. This could be due to the fact that the shorter glycans produced in the $GnTI^{-/-}$ cell line allow greater access of these still immature VRC01-like mAbs to the CD4-BS (LaBranche et al., 2018; Briney et al., 2016). The fourth, non-neutralizing antibody, P-p1e7, is the one lacking Glu_{96LC} (Figure S4B).

We concluded that the 426c Core immunogen elicits VRC01-like Abs that can recognize autologous and some heterologous soluble, stabilized Env trimers; avoiding clashes with variable regions 1, 2, and 3; and that the presence of $Glu96_{LC}$ appears to be important for these interactions. However, although these antibodies can avoid the glycans present on the V5 Env region, their binding is impaired by the glycan at position N276 in Loop D.

Antibodies Elicited by the 426c Core Accommodate the N276 Associated Glycans on Heterologous Env Cores

Plasma antibodies from 426c Core-immunized animals displayed CD4-BS-dependent recognition of heterologous monomeric WT Core proteins derived from the HxB2 (clade B), 45_01dH1 (clade B), 93TH057 (clade A/E), Q168a2 (clade A), and QH0692 (clade B) Envs (Figure S5A). These gp120-derived proteins lack the variable domains 1, 2, and 3, but harbor the N-X-T/S sequons at position N276 and in the V5 loop (Figure S5B). This observation suggested that the VRC01-like antibodies elicited by the 426c Core may bind heterologous Env Core proteins even in the presence of the N276-associated glycans.

The binding of the above-mentioned VRC01-like mAbs was examined to both the monomeric and the multimeric (C4b-based) forms of these Cores (Figure 4). The mAbs exhibited very weak binding to the monomeric form of HxB2, but not the other WT Cores (Figures 4A–4E). However, seven of eight mAbs tested bound the multimeric forms of the HxB2 and 45_01dH1 WT Core proteins (P-p1e7 that lacks Glu_{96LC} did not bind) (Figures 4F–4G), and one mAb (P-p3b3) also bound the multimeric forms of 93TH057 WT Core (Figure 4H), Q168a2 WT Core (Figure 4I), and QH0692 WT Core (Figure 4J). Mature VRC01 strongly recognized both the monomeric and multimerized forms of these Cores, while germline VRC01 did not recognize either. Hence, the 426c Core-elicited VRC01 antibodies display intermediate binding phenotypes in comparison to those of the germline and mature human VRC01 mAbs.

We conclude that a single immunization with the 426c Core elicits VRC01-like antibodies that can bypass the N276 glycans on heterologous Envs as long as the variable domains are absent (i.e., gp120-Core forms).

A Heterologous Boosting Immunization Improves the Binding Affinities of VRC01-like Antibodies to Env

Based on the above observations, we hypothesized that a boosting immunization with a heterologous Core Env expressing glycans at position N276 may expand the population of B cells that are capable of bypassing the N276-associated glycans. To test this hypothesis, a new group of animals were immunized first with the C4b nanoparticle form of 426c Core and 4 weeks later with the C4b nanoparticle form of the HxB2 WT Core Env. Env-specific B cells were isolated from the spleens and LNs 2 weeks following the boost immunization and analyzed as described above. A total of 160 eOD-GT8^{+}/eOD-GT8 KO^{-} B cells were isolated from these animals. 72 HCs and 79 LCs were successfully amplified and sequenced (Figure S2). The frequency of somatic mutation in the HC and LCs was higher in the antibodies isolated after the boost than after the prime (Figures 5A and S4).

Fifteen antibodies (IgG) were generated from paired VH/VL sequences displaying VRC01-class antibody features. These are designated by “B” to indicate they were isolated following the boost immunization. All mAbs recognized the 426c Core immunogen used during the prime in a CD4-BS-dependent manner (Figure 6A). They also bound eOD-GT8 in a VRC01 epitope-dependent manner (Figure 6B). While the VRC01-like antibodies elicited following the prime immunization displayed very weak binding to the monomeric HxB2 WT Core (Figure 4A), antibodies elicited after the boost, bound more strongly to several monomeric (Figures 6C–6G) and all multimeric WT Cores tested (Figure S6). Overall, the VRC01-like antibodies isolated after the boost have more mutations in both their HCs and LCs (Figure 5A), and higher binding affinities (Figures 5B and S7) than the antibodies isolated after the prime immunization.

One of the 15 antibodies (mAb B-p1b5) displayed binding to the 426c WT DS-SOSIP Env with an intact N276 glycan (Figure 6H). The binding was confirmed using negative stain (ns) electron microscopy (EM), where 1–3 Fabs can be observed bound per trimer (Figure 6I). A 3D nsEM reconstruction of 426c WT DS-SOSIP and B-p1b5 complex was generated in which coordinates of existing 426c DS-SOSIP D3 and glVRC01 (PDB: 6MYY) were fitted (Figure 6J) (Borst et al., 2018). Weak binding of a second mAb, B-p2e2, was also observed to the 426c WT DS-SOSIP Env. Importantly, out of the four mAbs tested for neutralization, B-p1b5 neutralized the WT 426c virus (IC_{50} of 32.05 μg/mL) expressed in GnTI$^{-/-}$ cells (Figure 6K). The human germline VRC01 mAb does not neutralize this virus, suggesting that our mouse antibody is one step farther in the evolutionary pathway to VRC01. B-p1b5 also displays neutralizing activity against the heterologous tier 2 virus CH0505TF when produced in GnTI$^{-/-}$ cells, when the loop D-associated 276 NLGS is absent (Table S2). The virus lacking 197, 276, 362, and 461/462 was neutralized, but the virus lacking only 197, 276, and 362 was not (Table S2). The neutralizing activity of B-p1b5 was abrogated by the D279K mutation (Table S2), as is the case for known human VRC01 antibodies suggesting that B-p1b5 recognizes the Env gp120 subunit in a VRC01-like

manner (Lynch et al., 2015). Thus, VRC01-like Abs isolated following the heterologous boost immunization have more mutations in their VH/VL domains, bind more efficiently to heterologous WT Core Envs than the antibodies isolated following the prime immunization with the 426c Core germline-targeting immunogen, and some also display autologous neutralization when the virus expresses Env with short glycans and heterologous tier 2 neutralizing activities, when certain NLGS surrounding the CD4-BS are absent. Thus, these antibodies have not yet matured sufficiently to become broadly neutralizing.

Vaccine-Elicited VRC01-like Antibodies Can Avoid Clashes with the N276-Associated Glycan

The results in the previous section suggested, but did not conclusively prove, that the VRC01-like Abs isolated following the prime and boost immunization with 426c Core and HxB2 WT Core could more efficiently circumvent the steric hindrance imposed by the glycan at position N276 than those antibodies isolated following the prime immunization with the “germline-targeting” 426c Core immunogen.

To address this point directly, we performed a series of complementary experiments. In one experiment, B-p1b5 was co-expressed in GnTI$^{-/-}$ cells with the 426c WT Core (which expresses the N-X-S/T sequon at position N276) as a disulfide cross-linked complex (Borst et al., 2018). The purified Ab-Env complex was further enzymatically treated with Endo H, and semiquantitative mass spectrometry analysis of the 276 NLGS was performed (Figure 7A). Man5 glycans were detected at position N276, confirming that B-p1b5 binds the 426c WT Core in the presence of N276-associated glycans. Despite the additional Endo H treatment following complex formation, no $(GlcNAc)_1$ glycopeptides were detected at the 276 NLGS by liquid chromatography-tandem mass spectrometry (LC-MS/MS). This observation validated that bound B-p1b5 antibody protected the N276 glycan from enzymatic digestion when interacting with its cognate epitope.

Additional experiments were performed to probe these interactions in the absence of disulfide cross-linking. In one such experiment, we used an N276-dependent mAb, 179NC75, to purify the N276-glycosylated HxB2 WT Core Env (Freund et al., 2015) (Figure 7B). Purified monomeric HxB2 WT Core expressed in GnTI$^{-/-}$ cells was incubated with 179NC75 immobilized on magnetic beads and the bound Core molecules were eluted and tested for recognition by mouse VRC01-like antibodies N-p4a9 and N-p3g9, isolated from unimmunized animals; P-p3b3, isolated following the prime immunization; and B-p1a11 and B-p1b5, isolated following the boost immunization. As expected, the antibodies isolated from unimmunized animals did not display HxB2 WT Core reactivity (Figures 7C and 7D). P-p3b3 displayed marginal reactivity to HxB2 WT Core molecules expressing N276 glycans (“enriched”) (Figure 7E), while the two antibodies isolated after the boost, bound strongly to the HxB2 WT Core molecules expressing N276 glycans (“enriched”) (Figures 7F and 7G).

In another set of experiments, monomeric 426c WT Core and HxB2 WT Core proteins expressed in GnTI$^{-/-}$ cells were incubated with magnetic beads coated with the above-mentioned mouse VRC01-like antibodies. Following immunoprecipitation, the flow-through and eluted materials were subjected to gel electrophoresis (Figures 7H and 7I). As expected,

neither 426c WT Core nor HxB2 WT Core proteins were immunoprecipitated by the N-p3g9 and N-p4a9 mAbs. 426c WT Core, but not HxB2 WT Core, was precipitated by P-p3b3. In contrast, both 426c WT Core and HxB2 WT Core were immunoprecipitated by B-p1b5. Semiquantitative mass spectrometry analysis was performed to determine the presence of Man5 glycans at position N276 in the immunoprecipitated material (Figures 7J and 7K). This analysis confirmed that the mouse VRC01-like antibodies isolated following the prime have the potential of recognizing 426c WT Core molecules expressing N276-associated glycans and that the antibodies isolated following the boost have the potential of recognizing both the 426c WT Core and HxB2 WT Core in the presence of N276 glycans. We note that these antibodies preferentially immunoprecipitated Env molecules lacking the N276-associated glycans, a consequence of not yet being fully matured following the prime-boost immunization scheme.

Collectively, the above experiments confirm that the VRC01-like antibodies isolated following the boost immunization can accommodate N276-associated glycans on fully glycosylated heterologous gp120-derived Core proteins, but less so on trimeric Envs present on virions.

DISCUSSION

A major challenge to the successful maturation of the germline forms of VRC01 antibodies toward their broadly neutralizing forms is the steric hindrance imposed by glycan molecules present on the conserved loop D 276 NLGS. As the present germline-targeting Env-based immunogens are designed to specifically lack the 276 NLGS (Jardine et al., 2013, 2015; McGuire et al., 2013, 2014, 2016; Medina-Ramírez et al., 2017), they are expected to preferentially activate BCRs that recognize the VRC01 epitope when N276-associated glycans are absent. Efforts to guide the maturation of such antibodies through sequential immunization with Env constructs also lacking 276 NLGS have so far met limited success (Briney et al., 2016; Tian et al., 2016). In the study by Tian et al., six different immunogens (only the fifth and sixth of which expressed N276-associated glycans) were sequentially administered in a knockin mouse model that expresses both the human IGHV1–2*02 and the germline human IGKV3–20*01 genes. mAbs isolated at the end of the immunization efficiently neutralized autologous 426c viruses lacking the N276 NLGS, and one antibody weakly neutralized the autologous 426c WT virus, which presumably had glycans occupying N276. The mechanism by which this mAb could bypass the N276-associated glycan was not reported (Tian et al., 2016). The study by Briney et al. was conducted in the same animal model we employed here, which we consider to be more stringent than the one employed by Tian, as only the glVRC01 HC is knocked in. Thus, in this model, the immunogens must first activate the rare B cells that also express a VRC01-like LC; i.e., one with 5-aa CDRL3s. Three different immunogens were administered sequentially, all three lacking N276-associated glycans. The antibodies isolated at the end of immunization efficiently neutralized heterologous viruses lacking N276-asociated glycans, and one antibody neutralized a tier 2 heterologous virus, although it is unclear whether all the virion-associated Envs express N276-associated glycans and whether and how this particular antibody bypassed the N276 glycan on this virus but not on the other viruses tested (Briney et al., 2016).

Here, we tested an alternative immunization scheme during which the prime immunization with the 426c Core germline-targeting immunogen is immediately followed by an immunization with a heterologous Core that expresses N276-associated glycans. This scheme was selected because we observed that a fraction of the VRC01-like antibodies elicited by the 426c Core immunogen display weak binding to heterologous Cores with N276 glycans. Indeed, the boost immunization improved the ability of the elicited VRC01-like antibodies to bypass the N276-associated glycans. Our observations are in agreement with reports by Escolano et al. (2016, 2019), where germline PGT121 BCRs were activated upon immunization with very low-affinity Env-derived immunogen.

The 426c Core immunogen selects for VRC01-like antibodies with key features. The H35N mutation in the CDRH1 domain leads to an increased stability between the CDRH1 and CDRH3 domains of the HC, whereas the selection of the $Glu96_{LC}$ allows for the formation of a hydrogen bond with $Gly459_{gp120}$ at the N terminus of the V5 region (West et al., 2012; Zhou et al., 2013). Our data indicate that, within the 5-aa-long CDRL3 domains, the presence of $Glu96_{LC}$ appears to be important for the antibody interactions with autologous and heterologous Core proteins. LCs with 5-aa-long CDRL3s are identifiable from naive B cells in this mouse model. However, we have not yet identified LCs with 5-aa-long CDRL3 containing a $Glu96_{LC}$ in the BCR repertoire analysis of naive B cells from the unimmunized mice. Either these LCs are present at extremely low frequencies and our germline-targeting immunogen selects for them, or $Glu96_{LC}$ is the result of somatic hypermutation (SHM) and subsequent selection in the germinal center following immunization with the 426c Core immunogen.

The majority of mouse VRC01-like antibodies elicited by the 426c Core, and which were subsequently boosted by the HxB2 WT Core, express LCs derived from the mouse k8–30*01 VL gene (Figures 1C and S4B), similar to what was previously reported during eOD-GT8-based immunizations in this same mouse model (Briney et al., 2016; Jardine et al., 2015). As a result, their CDRL1 are 17 aa's long (Figures 2 and S4B). Most mature human VRC01 mAbs express shorter CDRL1s (7–11 aa long, per Kabat numbering), which sometimes contain flexible glycine residues (Zhou et al., 2013). These CDRL1 features are believed to be necessary for the antibody LCs to accommodate the N276-associated glycans (Zhou et al., 2013). However, several glVRC01-class antibodies isolated from naive B cells using eOD-GT8 as a bait express longer CDRL1s (Havenar-Daughton et al., 2018; Jardine et al., 2016). One of them, VRC01c-HuGL2, recognizes eOD-GT8 in a manner similar to mature VRC01 (Jardine et al., 2016) and has a CDRL1 almost identical in aa sequence as the one present in the mouse VRC01 antibodies described here (Figure 2).

As compared to the rest of the VL domains, the CDRL1 regions appear to be under intense selective pressure to accumulate negatively charged aa's (Figure S4B). For instance, in most sequences, $Lys30_{LC}$ is replaced by a glutamic acid and additional negatively charged aa's (Asp or Glu) are also introduced in that same general region of CDRL1. Although we were able to confirm that the mouse VRC01-like antibodies elicited by our vaccination strategy recognize the VRC01 epitope in the presence of N276-associated glycans, the disordered CDRL1 structures limit our understanding on how the introduction of negatively charged aa's allow these LCs to accommodate these glycans. Affinity maturation of the antibodies

outside of the CDRL1 region may have compensated for the entropic cost of binding in the presence of the N276-associated glycan as has been observed in the VRC08 antibody lineage, which has a long rigid CDRL1 (Bonsignori et al., 2018). VRC01-like antibodies that do not express k8–30*01-derived VL domains were also isolated after the prime immunization (Figure S4B). These express shorter CDRL1 domains (10–11 aa's), but in contrast to the k8–30*01-expressing antibodies, they were not mutated from germline, nor did they contain Glu96. So far, the neutralizing activities of mAbs isolated following the prime-boost immunization are evident against the 426c-derived virus lacking the 276 NLGS and against the heterologous CH0505TF-derived virus that not only lacks the N276 NLGS but also V5-associated NLGS (positions 461/462) (Table S2). The observation that the D279K mutation abolished the neutralizing activity of mouse VRC01-like antibodies indicates that this activity is indeed targeting the VRC01 epitope. In that case, the absence of V5-associated NLGS appears to be required for neutralization. In all cases, the potency of neutralization was higher when the target virus was expressed in 293 GnTI$^{-/-}$ cells, an indication that the mouse VRC01-like antibodies have not yet accumulated the necessary mutations to accommodate complex glycans surrounding the CD4-BS. Presently, it is unknown whether further maturation of the mouse VRC01-like antibodies toward their broad neutralizing activities will be delayed by the presence of long CDRL1 domains.

Although approximately 0.08% of B cells express germline VRC01-like BCRs in the mouse model employed here (as compared to approximately 0.01% in humans), approximately 80% of the B cells express the already rearranged VDJ germline HC VRC01 chain (Jardine et al., 2015). It will therefore be important to evaluate the prime-boost immunization protocol discussed here, at more physiological frequencies of target B cells. Such experiments would most likely require adoptive transfer of target B cells into a wild-type animal, as recently reported (Abbott et al., 2018; Dosenovic et al., 2018).

The data presented here inform how VRC01-class antibody responses may be generated during natural HIV-1 infection. It suggests that although viral Env species that initiated the expansion of precursor VRC01-class BCRs in the context of infection may either lack N276-associated glycans or have short N276-associated glycans, the subsequent viral Envs that guide the maturation of these antibodies to bypass the N276-associated glycans most likely express glycans at N276. Indeed, sequence analysis of viral Envs in patient 45 (Lynch et al., 2015), from which VRC01 was isolated from (Wu et al., 2010), indicate the early presence of viral variants lacking N276-associated glycans, which were gradually replaced by viral Env variants expressing N276-associated glycans. Also, the recent report by Umotoy et al. (2019) suggests that in the context of HIV-1 infection the development of VRC01 bnAbs may benefit from an early B cell response to Envs with N276-associated glycans. In this last study, VRC01-class lineages with preferred reactivity in the presence of N276-associated glycans were also identified.

Our study informs on how to guide the maturation of glVRC01-class antibodies during immunization, so that the immunogens employed during the boost select for antibodies with mutations that allow them to accommodate the N276-associated glycan. As such, our results are relevant to current and upcoming clinical trials that evaluate the ability of germline-targeting immunogens to elicit cross-reactive VRC01-class antibody responses.

STAR★METHODS

LEAD CONTACT AND MATERIALS AVAILABILITY

Further information and requests for reagents should be directed to and will be fulfilled by Leonidas Stamatatos (lstamata@fredhutch.org). All reagents generated in this study can be made available upon request through Materials Transfer Agreements.

EXPERIMENTAL MODEL AND SUBJECT DETAILS

Immunizations were performed in the glH-VRC01 mouse (Jardine et al., 2015). It is heterozygous for the transgene (glVRC01 HC with the CDRH3 found in the mutated antibody) and only expresses mouse light chains. The Fred Hutch Institutional Animal Care and Use Committee approved all mouse studies. Mice were 6–12 weeks old at the beginning of the studies. Both male and female mice were included in these studies. Mice were immunized intramuscularly with a dose of 60 ug of protein and 60 ug of poly(I:C) (InvivoGen, Cat# tlrl-pic-5) split between the rear hind legs or with 50 ug of protein and 50 ul of GLA-LSQ (IDRI). Blood was collected retro-orbitally during immunization and via a cardiac puncture 2 weeks following the last immunization, at which time spleen and LNs were also harvested. Spleen and LNs were processed into a single cell suspension separately, frozen in FBS + 10% DMSO and stored in liquid nitrogen until further use. Blood, spleens and LNs were also isolated from non-immunized animals.

METHOD DETAILS

Protein expression and purification—Recombinant Env proteins expressed in nanoparticle (Ferritin or C4b-based) and NFL forms were expressed and purified as previously described (Guenaga et al., 2015; McGuire et al., 2016). Briefly, Envs were produced in 293E or 293F. Cell supernatants were purified by lectin affinity chromatography (*Galanthus nivalis*, Vector Labs), then subjected to Superdex 200 size exclusion chromatography (GE Healthcare). Ferritin nanoparticles underwent two rounds of size exclusion chromatography, first on a Superose 6 10/300GL column and then on a HiLoad 16/600 Superdex 200pg column.

Soluble trimeric SOSIP-based Envs were expressed and purified as previously described (Borst et al., 2018). In short, Env-expressing and furin-expressing plasmids were co-transfected (at 5:1 DNA ratio) into 293E cells. The Envs were purified from the cell supernatants using a Ni-affinity column followed by a Streptactin affinity column. Proteins were then subjected to enzymatic cleavage to remove the his-tag.

Monomeric proteins were produced by transfecting 293E or GnTI−/− cells with Env encoding plasmid. Cells are cultured for 6 days at 37°C, 5% CO_2, 80% humidity, and shaking at 125 RPM. Cells were centrifuged for 3000 RPM for 30 minutes and the supernatant sterile filtered through at 0.22 uM filter. Protein was purified by passing the cellular supernatant over a 5ml Fast Flow HisTrap column (Fisher Sci, Cat # 45000326). The eluted protein was purified on SEC as described above.

Core CD4-BS KO Env constructs contain the D368R and E370A mutations, while the eOD-GT8 KO contains the D368R mutation and the amino acids at positions 276–279 have been mutated to "NFTA."

Flow cytometry—Spleen and LN samples were thawed in a 37°C water bath until a small ice pellet remained in the tube and warm RPMI was then added dropwise. B cells were isolated using a mouse B cell isolation kit (EasySep, Cat#: 19854). If the antigen-specific cells were infrequent, an antigen enrichment protocol was used during which tetramers and decoys were first added to the cells and then anti-PE microbeads (Miltenyi Biotech Cat#: 130–048-801) and anti-APC microbeads (Miltenyi Biotech Cat#: 130–090-855) were added. Stained cells were then flowed over LS Columns (Miltenyi Biotec Cat#: 130–042-401) to separate the antigen-specific cells from the non-antigen specific. The B cells were then stained with a combination of the following antibodies: IgG1 FITC (BD Biosciences Cat#: 553443), IgG2b FITC (BD Biosciences Cat#: 553395), IgG2c FITC (Bio-Rad Cat#: STAR135F), IgG3 FITC (BD Biosciences Cat#: 553403), IgD PerCP-Cy5.5 (Biolegend Cat#: 405710), GL7 eFluor 450 (Thermo Fisher Scientific Cat#: 48–5902-80), eBioscience Fixable Viability Dye eFluor 506 (Thermo Fisher Scientific Cat#: 65–0866-14), CD3 BV510 (BD Biosciences Ct#: 563024), CD4 BV510 (BD Biosciences Cat#: 563106), Ly-6G/Ly-6C BV510 (BD Biosciences Cat#: 563040), F4/80 BV510 (BD Biosciences Cat#: 123135), IgM BV605 (Biolegend Cat#: 406523), B220 BV786 (BD Biosciences Cat#: 563894), CD38 AF700 (Thermo Fisher Scientific Cat#: 56–0381-82), CD19 BUV395 (BD Biosciences Cat#: 563557) or CD19 BV650 (BD BiosciencesCat#: 563235).The cells were stained with either 426c DMRS Core/426c DMRS DREA (D368R and E279A) Core or eOD-GT8/eOD-GT8 KO tetramers to select for Env specific and CD4-BS specific B cells. Tetramers were made by combining biotinylated Env with Streptavidin conjugated to either a PE or APC fluorophore (Prozyme, PJFS25 and PJ27S). From the groups of immunized mice, only samples from animals which showed eOD-GT8 plasma cross-reactivity were used for sorting.

Single B cell sorting—Naive, antigen-specific B cells were sorted as CD3−, CD4−, Gr-1−, F4/80−, B220+, CD19+, antigen+/antigen KO−. Class-switched IgG B cells from immunized animals were sorted based on the following markers: CD3−, CD4−, Gr-1−, F4/80−, B220+, CD19+, IgG1+, IgG2b+, IgG2c+, IgG3+, antigen+/antigen KO-. Individual B cells were sorted using the FACS ARIA II into a 96 well plate containing 20 ul of lysis buffer (20 U of RNase out (Thermo Fisher Scientific, Cat#: 10777019), 5 ul 5X Superscript IV RT buffer, 1.25 ul of 0.1M DTT, 0.625 ul of 10% Igepal, 13 ul nuclease free H_20) in each well. Plates with the sorted cells were stored at −80°C until further processing.

PCR amplification and sequencing of VH and VL genes—RNA was reverse transcribed to cDNA. For the reverse transcription reaction, 0.1 ul of Random Primers (3ug/ul, ThermoFisher Scientific Cat#: 48190011), 2 ul 10mM GeneAmp dNTP Blend (ThermoFisher Scientific, Cat#: N8080261), 1 ul SuperScript IV RT (200 U, ThermoFisher Scientific Cat#: 18090200), and 2.9 ul of nuclease free H_20 was added to the wells containing lysed cells. The reaction was run on a thermocycler for 10 minutes at 42°C, 10 minutes at 25°C, 60 minutes at 50°C, and 5 min at 94°C. Following reverse transcription, the

cDNA was diluted 1:2. Two rounds of PCR were employed to amplify both VH and VL genes. Each PCR reaction contains: 7 ul of cDNA, 2.4 units of HotStar Taq Plus (QIAGEN, Cat#: 203607), 240 nM of 5′ and 3′ primer, 350 uM GeneAmp dNTP Blend (Thermo Fisher Scientific, Cat#: N8080261), 4 ul of 10X buffer, and 27.8 ul nuclease free H_20. All primers and cycling conditions can be found in Tables S3 and S4. After the second round of PCR, samples were subjected to electrophoresis on a 1.5% agarose gel containing 0.1% Gel Red Nucleic Acid Stain (Biotium, Cat#: 41002). cDNA was purified using the enzyme ExoSap-IT (Affymetrix, Cat#: 78201). The purification reaction contained 5 ul of second round PCR product and 2 ul of ExoSap-IT. This reaction was run on a thermocycler for 15 min at 37°C followed by 15 min at 80°C. Following enzymatic purification, 5 ul of 5 uM second round 5′ primer was added to the sample and 3 ul of nuclease free water. Samples underwent sanger sequencing to identify the DNA sequence (Genewiz, Seattle, WA). Upon receiving the sequence, IMGT/V-QUEST was used to assign V, D, and J gene identity to the sequences and CDRL3 length (Brochet et al., 2008; Giudicelli et al., 2011). Sequences were included in the analysis (Figure S2) if they had an identifiable CDR3 region.

Amino acid mutations were identified by aligning the VH/VL gene sequences to the corresponding germline genes (IMGT Repertoire) using the Geneious Software (Version 8.1.9). For VL, mutations were counted beginning at the 5′ end of the V-gene to the 3′ end of the FW3. For VH, mutations were counted beginning at the 5′ end of the V-gene to the end of the KI gene. See Figure S4 for sequence alignments. To quantify the number of amino acid mutations, the sequence alignments were exported from Geneious and imported into R (Version 3.4.1) for analysis (R Core Team, 2018). This analysis uses the packages Biostrings (Pages et al., 2018), seqinr (Charif and Lobry, 2007), and tidyverse (Wickham, 2017). The sequences and code for this analysis can be found here: https://github.com/krparks/glVRC01_sequential_immunization.

VH and VL cloning and antibody expression—Gene-specific PCR was used to amplify the DNA product from the first round PCR using primers designed to anneal to the gene of interest as well as add ligation sites to facilitate insertion of the DNA fragment into the human IgG1 vector [ptt3 k for kappa (Snijder et al., 2018), and PMN 4–341 for gamma (Mouquet et al., 2010)]. Each gene specific PCR reaction contained 0.5 ul each of 10 uM 5′ and 3′ primer, 22.5 ul Accuprime Pfx Supermix (Cat#: 12344040), and 1.5 ul of 1st or 2nd round PCR product. The gene-specific PCR product was infused into the cut IgG1 vector in a reaction containing 12.5 ng of cut vector, 50 ng of insert, 0.5 ul of 5X Infusion enzyme (InFusion HD Cloning Kit, Cat#: 639649), and nuclease-free water to bring volume to 2.5 ul. The entire reaction was used to transform competent *E. coli* cells and plated on agar plates containing ampicillin. In some cases, gBlocks were synthesized to make the VH or VL containing plasmid (GenScript). 60 ng of glBlock was added to 15 ng of cut vector and 0.5 ul of 5× In-Fusion enzyme (Takara, Cat#: 1805251A). This reaction was run on the thermocycler for 15 min at 50°C. The entire reaction was used to transform competent *E. coli* cells (New England Biolabs, Cat#: C2987HI) and plated on agar plates containing ampicillin. Once a colony containing the insert sequence was identified, it was grown in LB broth containing ampicillin. DNA was prepared using QIAprep Spin Miniprep Kit (QIAGEN, Cat#: 27106). Equal amounts of heavy and light chain DNA and 293F

transfection reagent (Millipore Sigma, Cat#: 72181) were used to transfect 293E cells. 5–7 days post transfection cell supernatants were collected, and the antibodies were purified using Pierce Protein A agarose beads (Thermo Fisher Scientific, Cat#: 20334). The antibodies were eluted using 0.1 M Citric Acid into a tube containing 1 M Tris. The antibodies were buffer exchanged into 1XPBS using an amicon centrifugal filter.

To make Fabs, the IgG was cleaved overnight at 37°C to generate antigen binding fragment (Fab) with Endoproteinase Lys-C (NEB). To remove undigested IgG and IgG Fc fragments, the mixture was incubated with Protein A Agarose Resin for 1 hour at room temperature. Beads were washed with 1X PBS to remove excess Fab. Fab was further purified on SEC using a HiLoad 16/600 Superdex 200 pg (GE) column.

Protein Production for Structural Studies

P-p1f1Fab and eOD-GT8 (PDB ID: 6P8N): eOD-GT8 was expressed in HEK293S GnTI −/− cells. Cells were cultured in suspension and transfected using 500 μg eOD-GT8 plasmid with 293 Free Transfection Reagent (Novagen) in 1 L. After 6 days, cells were centrifuged at 4,500 rpm for 20 min and supernatant was filter-sterilized. A His-tag was utilized for purification by adding His60 Ni-Superflow Resin (Takara, Cat #:636660) in the supernatant at 4°C overnight. Ni Resin was washed with a solution of 150mM NaCl, 20 mM Tris pH 8.0, 20 mM Imidazole pH 7.0 and eluted with a solution of 300 mM NaCl, 50 mM Tris pH 8.0, 250 mM Imidazole pH 7.0. Protein was further purified using SEC as previously described. Complexes of eOD-GT8 and P-p1f1Fab were made by mixing equal molar ratio of both proteins for 1 hour at room temperature. Complexes were then mixed with Endo H (NEB, Cat#: P0702S) for 1hour at 37°C. SEC was used to remove any uncomplexed protein and Endo H. Complexes were concentrated to ~10 mg/mL for crystallization trials.

P-p3b3Fab and 426c Core (PDB ID: 6P8M): P-p3b3Fab crosslinked to 426c Core was expressed in HEK293S GnTI−/− cells. Cells were cultured in suspension and transfected with equal parts of 426c Core G459C, P-p3b3Fab-A60C heavy chain, and P-p3b3 light chain plasmids (500 μg total/L) as previously described (Borst et al., 2018). Complexes were purified with a His tag on the Fab heavy chain C terminus followed by SEC to remove nonspecific proteins and excess unliganded Fab. An SDS gel was run on the complex to confirm the disulfide bond formation between the P-p3b3fab and the 426c Core. Complexes were treated with EndoH (New England Biolabs, Cat#: P0702S) for 1hr at 37°C and run on SEC to remove Endo H. Complexes were concentrated to ~10 mg/mL for crystallization trials.

Crystallization—Crystallization conditions were screened and monitored with an NT8 drop setter and Rock Imager (Formulatrix). Screening was done with Rigaku Wizard Precipitant Synergy block no. 2 (MD15-PS-B), Molecular Dimensions Proplex screen HT-96 (MD1–38), and Hampton Research Crystal Screen HT (HR2–130) using the sitting drop vapor diffusion method. P-p1f1fab + eOD-GT8 crystals were further optimized with hanging drop trays using vapor diffusion method. Final crystals for P-p1f1fab + eODGT8 were grown in 22.5% PEG 3350, 13.5% Isopropanol, 0.18M Ammonium Citrate pH 4.0. Final crystals for P-p3b3fab + 426c Core were grown in 0.67% PEG 4000, 0.67M

Ammonium Citrate pH 5.5. P-p1f1fab + eODGT8 crystal were cryo protected in a solution of 20% molar excess of the crystallization condition and 20% Ethylene Glycol. P-p3b3fab + 426c Core were cryoprotected in the original crystallization condition. P-p3b3fab + 426c Core and P-p1f1fab + eODGT8 were sent to ALS 5.0.2 and diffraction data was collected to 3.59 Å and 3.2 Å respectively. Data were processed using HKL2000 (Otwinowski and Minor, 1997).

Structure Solution and Refinement—The structure of P-p1f1Fab + eOD-GT8 was solved by molecular replacement using PDB ID: 4JPK as a search model in Phaser in Phenix. The structure of P-p3b3Fab + 426c Core was solved by molecular replacement using PDB ID: 6MFT as a search. The structures were further refined with COOT (Emsley and Cowtan, 2004) and Phenix (Adams et al., 2004). The refinement statistics are summarized in Table S1.

Negative-stain EM—The 426c WT DS-SOSIP/B-p1b5 complex was formed by co-incubating B-p1b5 Fab to 426c WT DS-SOSIP trimer at a 2:1 B-p1b5:gp120 monomer ratio (alternatively referred to as 6:1 B-p1b5 trimer ratio) ratio for 10 minutes at 4°C. Samples treated with glutaraldehyde were cross-linked in 0.25% GTA for 45 s followed by quenching with 1M Tris, followed by purification of bound complexes via a Superdex 200 10/300 GL Increase column. 426c WT DS-SOSIP/B-p1b5 Fab complexes examined in this study (3 μL) were negatively stained at a final concentration of 0.010 mg/mL using Gilder Grids overlaid with a thin layer of carbon and 2% uranyl formate (Electron Microscopy Sciences, Cat#: 22451) as previously described (Veesler et al., 2014).

Data were collected on an FEI Technai 12 Spirit 120kV electron microscope equipped with a Gatan Ultrascan 4000 CCD camera. A total of ~300 images were collected per sample by using a random defocus range of 1.1–2.0 μm with a total exposure of 45 e^{-}/A^{2}. Data were automatically acquired using Leginon (Suloway et al., 2005) and data processing was carried out using Appion (Lander et al., 2009). The parameters of the contrast transfer function (CTF) were estimated using CTFFIND4 (Mindell and Grigorieff, 2003), and particles were picked in a reference-free manner using DoG picker (Voss et al., 2009). Particles were extracted with a binning factor of 2 after correcting for the effect of the CTF by flipping the phases of each micrograph with EMAN 1.9 (Ludtke et al., 1999). The GTA cross-linked 426c WT DS-SOSIP B-p1b5 Fab stack was pre-processed in RELION/2.1 (Kimanius et al., 2016; Scheres, 2012a, 2012b) with an additional binning factor of 2 applied, resulting in a final pixel size of 6.4 Å. Resulting particles were sorted by reference-free 2D classification over 25 iterations. The best particles were chosen for 3D classification into 2 classes using C1 symmetry in RELION/2.1 (Kimanius et al., 2016). The best class of particles were refined using Relion/3.0 (Zivanov et al., 2018).

Biolayer Interferometry (BLI)—Antibody binding to recombinant Env proteins was determined using biolayer interferometry on the Octet Red 96 (ForteBio, Inc, Menlo Park, CA), as previously described (Yacoob et al., 2016). Briefly, anti-human Fc capture biosensors (ForteBio, Cat#: 18–5063) were activated by immersion into 1× Kinetics Buffer (1× PBS, 0.1% BSA, 0.02% Tween-20, 0.005% NaN_3) for 10 minutes. Antibodies were loaded onto an anti-human Fc capture probe at 20 ug/ml. The probes were then dipped into

solutions containing recombinant Env: 2 uM for monomeric gp120-derived Envs or 1 uM for C4b and trimeric Env (SOSIP or NFL designs). Parameters for all BLI assays were: 30 s of baseline measurement, 240 s to load the antibody onto the anti-human Fc capture probe, 60 s of baseline measurement, 300 s of association, 300 s of dissociation. All measurements of Env-Ab binding were corrected by subtracting the background signal obtained from env traces generated with an irrelevant negative control IgG.

Kinetic analyses were performed by BLI as described above using recombinant Fabs loaded onto FAB2G biosensors (ForteBio, Cat#: 18–5126) (@ 40 ug/ in 1XPBS) and 2-fold dilutions of envelope monomers (ranging from 50 uM - 391 nM), and by extending the dissociation phase of binding to 600 s. Curve fitting was used to determine relative apparent antibody affinities for envelope using a 1:1 binding model and the data analysis software (ForteBio). Mean k_{on}, k_{off}, and K_D values were determined by averaging all binding curves within a dilution series having R^2 values of greater than 95% confidence level.

Enzyme linked immunosorbent assays—Plasma samples were heated inactivated at 56°C for 1 hour, centrifuged at 13,000 for 10 min and stored at 4°C or −20°C. ELISAs were done in either a half-area 96 well or 384 well plate format. For a 384 well plate ELISA, 30 ul of protein at 0.1 uM in coating buffer (0.1M sodium bicarbonate, pH: 9.4–9.6) was added to each well and incubated a room temperature overnight. Plates were washed 4× with ELISA wash buffer (1XPBS + 0.2% Tween-20). 80 ul of blocking buffer (1X PBS + 10% non-fat milk + 0.03% Tween20) was added to the plates and they were incubated at 37°C for 1–2 hours. Plates were then washed 4× with ELISA wash buffer. Plasma was diluted 1:10 in blocking buffer and diluted 1:3 across or down the plate. His tag control started at 1 μg/ml. The plates were incubated for 1 hour at 37°C. The plates were washed 4× with ELISA was buffer. 30 ul of secondary antibody was added to each well. The plates were incubated for an hour at 37°C. Plates were washed 4× with ELISA wash buffer. Following washing 30 ul of SureBlue Reserve TMB Microwell Peroxidase Substrate: KPL (Cat #: 53–00-02) was added to each well. The plates were incubated for 5 minutes at room temperature. 30 ul of 1N H_2SO_4 was added to each well. Plates were read immediately on the SpectraMax M2 microplate reader (Molecular Devices) at 450 nm. Blank wells were used to subtract the background signal in the analysis. 96 well plate ELISAs followed a similar protocol but used 50 ul of volume for the coating of protein, dilution volumes, secondary antibody volume, and development steps. 120 ul of blocking buffer was used to block the plates.

Neutralization assays—Neutralizing antibody activity was measured in 96-well culture plates by using Tat-regulated luciferase (Luc) reporter gene expression to quantify reductions in virus infection in TZM-bl cells. TZM-bl cells were obtained from the NIH AIDS Research and Reference Reagent Program, as contributed by John Kappes and Xiaoyun Wu. Assays were performed with HIV-1 Env-pseudotyped viruses as described previously (Montefiori, 2009). For the assays, mAbs were used at 100 ug/ml or the highest concentration possible. Samples were then diluted over seven 3-fold dilutions and pre-incubated with virus (~150,000 relative light unit equivalents) for 1 hr at 37°C before addition of cells. Following an additional 48 hr incubation, cells were lysed and Luc activity determined using a microtiter plate luminometer and BriteLite Plus Reagent (PerkinElmer,

Cat#: 6066766). Neutralization titers are the antibody concentration at which relative luminescence units (RLU) were reduced by 50% compared to RLU in virus control wells after subtraction of background RLU in cell control wells.

Immunoprecipitation—Purified recombinant IgGs were covalently coupled to MyOne Tosylactivated Dynabeads (Thermo Fisher Scientific, Cat#: 65501). Coupling and Env-immunoprecipitation were carried out according to the manufacturer's protocol. Briefly, 5 mg of Env produced in HEK293S GnTI$^{-/-}$ were incubated with 200 μg of IgG-beads for 30 min. The IgG-Env protein complexes were then precipitated using magnetic separation and washed 3–4× before performing acidic elution and pH neutralization of the bound material. Env-samples of the original input of 426c WT Core or HxB2 WT Core, and bead-bound/eluted and unbound fractions were subjected to SDS gel electrophoresis under reducing conditions. A sample of the bound fractions were subjected to LC-MS/MS analysis or used for BLI.

Mass spectrometry—For analysis of the *N*-linked glycosylation profile of the cross-linked 426c WT Core-P1B5 complex, 250 pmol of sample was denatured, reduced, and alkylated by dilution to 5 μM in 50 μL of buffer containing 100 mM Tris (pH 8.5), 10 mM Tris (2-carboxyethylphosphine (TCEP), 40 mM iodoacetamide or 40 mM iodoacetic acid, and 2% (wt/vol) sodium deoxycholate. Samples were first heated to 95°C for 5 min and then incubated for an additional 25 min at room temperature in the dark. The samples were digested with trypsin (Thermo Fisher Scientific, Cat#: 90057), by diluting 20 μL of sample to a total volume of 100 μL of buffer containing 50 mM ammonium bicarbonate (pH 8.5). Trypsin was added in a ratio of 1:50 (w/w) before incubation at 37°C overnight. Subsequently, 2 μL of formic acid was added to precipitate the sodium deoxycholate from the solution. Following centrifugation at 17,000 × g for 25 min, 85 μL of the supernatant was collected and centrifuged again at 17,000 × g for 5 min to ensure removal of any residual precipitated deoxycholate. 80 μL of this supernatant was collected. For each sample, 8 μL was injected on a Thermo Scientific Orbitrap Fusion Tribrid mass spectrometer. A 35 cm analytical column and a 3 cm trap column filled with ReproSil-Pur C18AQ 5 μM (Dr. Maisch) beads were used. Nanospray LC-MS/MS was used to separate peptides over a 90 min gradient from 5% to 30% acetonitrile with 0.1% formic acid. A positive spray voltage of 2100 was used with an ion transfer tube temperature of 350°C. An electron-transfer/higher-energy collision dissociation ion-fragmentation scheme (Frese et al., 2013) was used with calibrated charge-dependent entity-type definition parameters and supplemental higher-energy collision dissociation energy of 0.15. A resolution setting of 120,000 with an AGC target of 2×10^5 was used for MS1, and a resolution setting of 30,000 with an AGC target of 1×10^5 was used for MS2. Data were searched with the Protein Metrics Byonic software (Bern et al., 2012), using a small custom database of recombinant protein sequences including the proteases used to prepare the glycopeptides. Reverse decoy sequences were also included in the search. Specificity of the search was set to C-terminal cleavage at R/K (trypsin), allowing up to three missed cleavages, with EthcD fragmentation (b/y- and c/z-type ions). We used a precursor mass and product mass tolerance of 12 ppm and 24 ppm, respectively. Carbamidomethylation of cysteines was set as fixed modification, carbamidomethylation of lysines was set as a variable modification, methionine oxidation as

variable modification, and a concatenated N-linked glycan database (derived from the four software-included databases) was used to identify glycopeptides. All analyzed glycopeptide hits were manually inspected to ensure their quality and accuracy.

Semiquantitative LC-MS/MS of P-p3b3, B-p1b5 and VRC01-immunoprecipitation experiments were performed using Skyline (MacLean et al., 2010) with peak integration and LC-MS/MS searches imported from Byonic, as previously described (Borst et al., 2018). Missed cleavages and post-translational modifications listed above for qualitative LC-MS/MS searches were included in the quantification of glycopeptides. All MS1 peak areas used for integration were manually inspected. Each fraction was performed as part of two technical replicates and was subsequently averaged. Calculations and plots for glycoform enrichment graphs were generated by subtracting the relative signal values of the input Core fraction from the unbound or bound Core fractions.

QUANTIFICATION AND STATISTICAL ANALYSIS

Mean and standard deviations were calculated using R (Version 3.4.1). Statistical analyses were calculated using R (Version 3.4.1) (R Core Team, 2018) and GraphPad Prism. Descriptions of the statistical methods used for each dataset are described in the figure legends. The tidyverse packages (Wickham, 2017) were used in R to manipulate data and create graphs in addition to GraphPad Prism.

DATA AND CODE AVAILABILITY

The sequences of mAbs reported here have been deposited on GenBank and in the GitHub respository: https://github.com/krparks/glVRC01_sequential_immunization. The accession numbers of the mAb sequences are GenBank: MN087228 - MN087315 (Table S5). Multimeric and monomeric heterologous Env sequences have been deposited on GenBank, accession numbers GenBank: MN179660-MN179671 (Table S5). Coordinates and structure factors have been deposited on the Protein Data Bank under PDB: 6P8N and PDB: 6P8M. Raw and analyzed Mass Spectrometry data have been deposited on PRIDE. The accession number for the mass spectrometry data is PRIDE: PXD015168.

Supplementary Material

Refer to Web version on PubMed Central for supplementary material.

ACKNOWLEDGMENTS

We acknowledge Claire Levy and Pavitra Roychoudhury for help with somatic hypermutation analysis. This study was supported by NIH grants R01 AI104384, P01 AI138212, and U19 AI109632 (to L.S.), NIH contract HHSN272201800004C (to D.C.M.), and R01GM120553 (to D.V.); as well as by a Pew Biomedical Scholars Award from the Pew Charitable Trust and an Investigators in the Pathogenesis of Infectious Disease Award from the Burroughs Wellcome Fund (to D.V.). This work was also supported by the Arnold and Mabel Beckman Cryo-EM Center at the University of Washington and the Proteomics Resource (UWPR95794). We thank the J.B. Pendleton Charitable Trust for its generous support of Formulatrix robotic instruments. X-ray diffraction data were collected at the Berkeley Center for Structural Biology beamline 5.0.2, which is supported in part by the National Institute of General Medical Sciences. The Advanced Light Source is supported by the Director, Office of Science, Office of Basic Energy Sciences, of the United States Department of Energy under contract DE-AC02-05CH11231.

REFERENCES

Abbott RK, Lee JH, Menis S, Skog P, Rossi M, Ota T, Kulp DW, Bhullar D, Kalyuzhniy O, Havenar-Daughton C, et al. (2018). Precursor frequency and affinity determine B cell competitive fitness in germinal centers, tested with germline-targeting HIV vaccine immunogens. Immunity 48, 133–146.e6. [PubMed: 29287996]

Adams PD, Gopal K, Grosse-Kunstleve RW, Hung L-W, Ioerger TR, McCoy AJ, Moriarty NW, Pai RK, Read RJ, Romo TD, et al. (2004). Recent developments in the PHENIX software for automated crystallographic structure determination. J. Synchrotron Radiat 11, 53–55. [PubMed: 14646133]

Arnaout R, Lee W, Cahill P, Honan T, Sparrow T, Weiand M, Nusbaum C, Rajewsky K, and Koralov SB (2011). High-resolution description of antibody heavy-chain repertoires in humans. PLoS ONE 6, e22365. [PubMed: 21829618]

Balazs AB, Ouyang Y, Hong CM, Chen J, Nguyen SM, Rao DS, An DS, and Baltimore D (2014). Vectored immunoprophylaxis protects humanized mice from mucosal HIV transmission. Nat. Med 20, 296–300. [PubMed: 24509526]

Bern M, Kil YJ, and Becker C (2012). Byonic: advanced peptide and protein identification software. Curr. Protoc. Bioinformatics Chapter 13, Unit 13.20.

Bonsignori M, Zhou T, Sheng Z, Chen L, Gao F, Joyce MG, Ozorowski G, Chuang G-Y, Schramm CA, Wiehe K, et al.; NISC Comparative Sequencing Program (2016). Maturation pathway from germline to broad HIV-1 neutralizer of a CD4-mimic antibody. Cell 165, 449–463. [PubMed: 26949186]

Bonsignori M, Scott E, Wiehe K, Easterhoff D, Alam SM, Hwang K-K, Cooper M, Xia S-M, Zhang R, Montefiori DC, et al. (2018). Inference of the HIV-1 VRC01 antibody lineage unmutated common ancestor reveals alternative pathways to overcome a key glycan barrier. Immunity 49, 1162–1174.e8. [PubMed: 30552024]

Borst AJ, Weidle CE, Gray MD, Frenz B, Snijder J, Joyce MG, Georgiev IS, Stewart-Jones GB, Kwong PD, McGuire AT, et al. (2018). Germline VRC01 antibody recognition of a modified clade C HIV-1 envelope trimer and a glycosylated HIV-1 gp120 core. eLife 7, e37688. [PubMed: 30403372]

Briney B, Sok D, Jardine JG, Kulp DW, Skog P, Menis S, Jacak R, Kalyuzhniy O, de Val N, Sesterhenn F, et al. (2016). Tailored immunogens direct affinity maturation toward HIV neutralizing antibodies. Cell 166, 1459–1470.e11. [PubMed: 27610570]

Brochet X, Lefranc M-P, and Giudicelli V (2008). IMGT/V-QUEST: the highly customized and integrated system for IG and TR standardized V-J and V-D-J sequence analysis. Nucleic Acids Res. 36, W503–W508. [PubMed: 18503082]

Burton DR, and Hangartner L (2016). Broadly neutralizing antibodies to HIV and their role in vaccine design. Annu. Rev. Immunol 34, 635–659. [PubMed: 27168247]

Charif D, and Lobry JR (2007). SeqinR 1.0–2: a contributed package to the R Project for statistical computing devoted to biological sequences retrieval and analysis In Structural Approaches to Sequence Evolution: Molecules, Networks, Populations, Bastolla U, Porto M, Roman E, and Vendruscolo M, eds. (Springer), pp. 207–232.

DeKosky BJ, Kojima T, Rodin A, Charab W, Ippolito GC, Ellington AD, and Georgiou G (2015). In-depth determination and analysis of the human paired heavy- and light-chain antibody repertoire. Nat. Med 21, 86–91. [PubMed: 25501908]

Doria-Rose NA, Schramm CA, Gorman J, Moore PL, Bhiman JN, DeKosky BJ, Ernandes MJ, Georgiev IS, Kim HJ, Pancera M, et al.; NISC Comparative Sequencing Program (2014). Developmental pathway for potent V1V2-directed HIV-neutralizing antibodies. Nature 509, 55–62. [PubMed: 24590074]

Dosenovic P, von Boehmer L, Escolano A, Jardine J, Freund NT, Gitlin AD, McGuire AT, Kulp DW, Oliveira T, Scharf L, et al. (2015). Immunization for HIV-1 broadly neutralizing antibodies in human Ig knockin mice. Cell 161, 1505–1515. [PubMed: 26091035]

Dosenovic P, Kara EE, Pettersson A-K, McGuire AT, Gray M, Hartweger H, Thientosapol ES, Stamatatos L, and Nussenzweig MC (2018). Anti-HIV-1 B cell responses are dependent on B cell

precursor frequency and antigen-binding affinity. Proc. Natl. Acad. Sci. USA 115, 4743–4748. [PubMed: 29666227]

Emsley P, and Cowtan K (2004). Coot: model-building tools for molecular graphics. Acta Crystallogr. D Biol. Crystallogr 60, 2126–2132. [PubMed: 15572765]

Escolano A, Steichen JM, Dosenovic P, Kulp DW, Golijanin J, Sok D, Freund NT, Gitlin AD, Oliveira T, Araki T, et al. (2016). Sequential immunization elicits broadly neutralizing anti-HIV-1 antibodies in Ig knockin mice. Cell 166, 1445–1458.e12. [PubMed: 27610569]

Escolano A, Gristick HB, Abernathy ME, Merkenschlager J, Gautam R, Oliveira TY, Pai J, West AP Jr., Barnes CO, Cohen AA, et al. (2019). Immunization expands B cells specific to HIV-1 V3 glycan in mice and macaques. Nature 570, 468–473. [PubMed: 31142836]

Frese CK, Zhou H, Taus T, Altelaar AFM, Mechtler K, Heck AJR, and Mohammed S (2013). Unambiguous phosphosite localization using electron-transfer/higher-energy collision dissociation (EThcD). J. Proteome Res 12, 1520–1525. [PubMed: 23347405]

Freund NT, Horwitz JA, Nogueira L, Sievers SA, Scharf L, Scheid JF, Gazumyan A, Liu C, Velinzon K, Goldenthal A, et al. (2015). A new glycan-dependent CD4-binding site neutralizing antibody exerts pressure on HIV-1 in vivo. PLoS Pathog. 11, e1005238. [PubMed: 26516768]

Gautam R, Nishimura Y, Pegu A, Nason MC, Klein F, Gazumyan A, Golijanin J, Buckler-White A, Sadjadpour R, Wang K, et al. (2016). A single injection of anti-HIV-1 antibodies protects against repeated SHIV challenges. Nature 533, 105–109. [PubMed: 27120156]

Giudicelli V, Brochet X, and Lefranc M-P (2011). IMGT/V-QUEST: IMGT Standardized analysis of the immunoglobulin (IG) and T cell receptor (TR) nucleotide sequences. Cold Spring Harb. Protoc 2011, 695–715. [PubMed: 21632778]

Guenaga J, Dubrovskaya V, de Val N, Sharma SK, Carrette B, Ward AB, and Wyatt RT (2015). Structure-guided redesign increases the propensity of HIV Env to generate highly stable soluble trimers. J. Virol 90, 2806–2817. [PubMed: 26719252]

Havenar-Daughton C, Sarkar A, Kulp DW, Toy L, Hu X, Deresa I, Kalyuzhniy O, Kaushik K, Upadhyay AA, Menis S, et al. (2018). The human naive B cell repertoire contains distinct subclasses for a germline-targeting HIV-1 vaccine immunogen. Sci. Transl. Med 10, eaat0381. [PubMed: 29973404]

Hofmeyer T, Schmelz S, Degiacomi MT, Dal Peraro M, Daneschdar M, Scrima A, van den Heuvel J, Heinz DW, and Kolmar H (2013). Arranged sevenfold: structural insights into the C-terminal oligomerization domain of human C4b-binding protein. J. Mol. Biol 425, 1302–1317. [PubMed: 23274142]

Hoot S, McGuire AT, Cohen KW, Strong RK, Hangartner L, Klein F, Diskin R, Scheid JF, Sather DN, Burton DR, and Stamatatos L (2013). Recombinant HIV envelope proteins fail to engage germline versions of anti-CD4bs bNAbs. PLoS Pathog. 9, e1003106. [PubMed: 23300456]

Jardine J, Julien J-P, Menis S, Ota T, Kalyuzhniy O, McGuire A, Sok D, Huang P-S, MacPherson S, Jones M, et al. (2013). Rational HIV immunogen design to target specific germline B cell receptors. Science 340, 711–716. [PubMed: 23539181]

Jardine JG, Ota T, Sok D, Pauthner M, Kulp DW, Kalyuzhniy O, Skog PD, Thinnes TC, Bhullar D, Briney B, et al. (2015). HIV-1 VACCINES. Priming a broadly neutralizing antibody response to HIV-1 using a germline-targeting immunogen. Science 349, 156–161. [PubMed: 26089355]

Jardine JG, Kulp DW, Havenar-Daughton C, Sarkar A, Briney B, Sok D, Sesterhenn F, Ereño-Orbea J, Kalyuzhniy O, Deresa I, et al. (2016). HIV-1 broadly neutralizing antibody precursor B cells revealed by germline-targeting immunogen. Science 351, 1458–1463. [PubMed: 27013733]

Joyce MG, Georgiev IS, Yang Y, Druz A, Geng H, Chuang G-Y, Kwon YD, Pancera M, Rawi R, Sastry M, et al. (2017). Soluble prefusion closed DS-SOSIP.664-Env trimers of diverse HIV-1 strains. Cell Rep. 21, 2992–3002. [PubMed: 29212041]

Kanekiyo M, Wei C-J, Yassine HM, McTamney PM, Boyington JC, Whittle JRR, Rao SS, Kong W-P, Wang L, and Nabel GJ (2013). Self-assembling influenza nanoparticle vaccines elicit broadly neutralizing H1N1 antibodies. Nature 499, 102–106. [PubMed: 23698367]

Kimanius D, Forsberg BO, Scheres SH, and Lindahl E (2016). Accelerated cryo-EM structure determination with parallelisation using GPUs in RELION-2. eLife 5, e18722. [PubMed: 27845625]

Kwong PD, and Mascola JR (2018). HIV-1 vaccines based on antibody identification, B cell ontogeny, and epitope structure. Immunity 48, 855–871. [PubMed: 29768174]

LaBranche CC, McGuire AT, Gray MD, Behrens S, Kwong PDK, Chen X, Zhou T, Sattentau QJ, Peacock J, Eaton A, et al. (2018). HIV-1 envelope glycan modifications that permit neutralization by germline-reverted VRC01-class broadly neutralizing antibodies. PLoS Pathog. 14, e1007431. [PubMed: 30395637]

Lander GC, Stagg SM, Voss NR, Cheng A, Fellmann D, Pulokas J, Yoshioka C, Irving C, Mulder A, Lau PW, et al. (2009). Appion: an integrated, database-driven pipeline to facilitate EM image processing. J. Struct. Biol 166, 95–102. [PubMed: 19263523]

Liao H-X, Lynch R, Zhou T, Gao F, Alam SM, Boyd SD, Fire AZ, Roskin KM, Schramm CA, Zhang Z, et al.; NISC Comparative Sequencing Program (2013). Co-evolution of a broadly neutralizing HIV-1 antibody and founder virus. Nature 496, 469–476. [PubMed: 23552890]

Ludtke SJ, Baldwin PR, and Chiu W (1999). EMAN: semiautomated software for high-resolution single-particle reconstructions. J. Struct. Biol 128, 82–97. [PubMed: 10600563]

Lynch RM, Wong P, Tran L, O'Dell S, Nason MC, Li Y, Wu X, and Mascola JR (2015). HIV-1 fitness cost associated with escape from the VRC01 class of CD4 binding site neutralizing antibodies. J. Virol 89, 4201–4213. [PubMed: 25631091]

MacLean B, Tomazela DM, Shulman N, Chambers M, Finney GL, Frewen B, Kern R, Tabb DL, Liebler DC, and MacCoss MJ (2010). Skyline: an open source document editor for creating and analyzing targeted proteomics experiments. Bioinformatics 26, 966–968. [PubMed: 20147306]

McGuire AT, Hoot S, Dreyer AM, Lippy A, Stuart A, Cohen KW, Jardine J, Menis S, Scheid JF, West AP, et al. (2013). Engineering HIV envelope protein to activate germline B cell receptors of broadly neutralizing anti-CD4 binding site antibodies. J. Exp. Med 210, 655–663. [PubMed: 23530120]

McGuire AT, Dreyer AM, Carbonetti S, Lippy A, Glenn J, Scheid JF, Mouquet H, and Stamatatos L (2014). HIV antibodies. Antigen modification regulates competition of broad and narrow neutralizing HIV antibodies. Science 346, 1380–1383. [PubMed: 25504724]

McGuire AT, Gray MD, Dosenovic P, Gitlin AD, Freund NT, Petersen J, Correnti C, Johnsen W, Kegel R, Stuart AB, et al. (2016). Specifically modified Env immunogens activate B-cell precursors of broadly neutralizing HIV-1 antibodies in transgenic mice. Nat. Commun 7, 10618. [PubMed: 26907590]

Medina-Ramírez M, Garces F, Escolano A, Skog P, de Taeye SW, Del Moral-Sanchez I, McGuire AT, Yasmeen A, Behrens A-J, Ozorowski G, et al. (2017). Design and crystal structure of a native-like HIV-1 envelope trimer that engages multiple broadly neutralizing antibody precursors in vivo. J. Exp. Med 214, 2573–2590. [PubMed: 28847869]

Mindell JA, and Grigorieff N (2003). Accurate determination of local defocus and specimen tilt in electron microscopy. J. Struct. Biol 142, 334–347. [PubMed: 12781660]

Montefiori DC (2009). Measuring HIV neutralization in a luciferase reporter gene assay. Methods Mol. Biol 485, 395–405. [PubMed: 19020839]

Mouquet H, Scheid JF, Zoller MJ, Krogsgaard M, Ott RG, Shukair S, Artyomov MN, Pietzsch J, Connors M, Pereyra F, et al. (2010). Polyreactivity increases the apparent affinity of anti-HIV antibodies by heteroligation. Nature 467, 591–595. [PubMed: 20882016]

Ogun SA, Dumon-Seignovert L, Marchand J-B, Holder AA, and Hill F (2008). The oligomerization domain of C4-binding protein (C4bp) acts as an adjuvant, and the fusion protein comprised of the 19-kilodalton merozoite surface protein 1 fused with the murine C4bp domain protects mice against malaria. Infect. Immun 76, 3817–3823. [PubMed: 18474650]

Otwinowski Z, and Minor W (1997). Processing of X-ray diffraction data collected in oscillation mode. Methods Enzymol. 276, 307–326.

Pages H, Aboyoun P, Gentleman R, and DebRoy S (2018). Biostrings: efficient manipulation of biological strings. http://bioconductor.org/packages/release/bioc/html/Biostrings.html.

Pegu A, Yang ZY, Boyington JC, Wu L, Ko S-Y, Schmidt SD, McKee K, Kong W-P, Shi W, Chen X, et al. (2014). Neutralizing antibodies to HIV-1 envelope protect more effectively in vivo than those to the CD4 receptor. Sci. Transl. Med 6, 243ra88.

R Core Team (2018). R: The R Project for Statistical Computing. https://www.R-project.org/.

Scheid JF, Mouquet H, Ueberheide B, Diskin R, Klein F, Oliveira TYK, Pietzsch J, Fenyo D, Abadir A, Velinzon K, et al. (2011). Sequence and structural convergence of broad and potent HIV antibodies that mimic CD4 binding. Science 333, 1633–1637. [PubMed: 21764753]

Scheres SHW (2012a). A Bayesian view on cryo-EM structure determination. J. Mol. Biol 415, 406–418. [PubMed: 22100448]

Scheres SHW (2012b). RELION: implementation of a Bayesian approach to cryo-EM structure determination. J. Struct. Biol 180, 519–530. [PubMed: 23000701]

Shingai M, Donau OK, Plishka RJ, Buckler-White A, Mascola JR, Nabel GJ, Nason MC, Montefiori D, Moldt B, Poignard P, et al. (2014). Passive transfer of modest titers of potent and broadly neutralizing anti-HIV monoclonal antibodies block SHIV infection in macaques. J. Exp. Med 211, 2061–2074. [PubMed: 25155019]

Snijder J, Ortego MS, Weidle C, Stuart AB, Gray MD, McElrath MJ, Pancera M, Veesler D, and McGuire AT (2018). An antibody targeting the fusion machinery neutralizes dual-tropic infection and defines a site of vulnerability on Epstein-Barr virus. Immunity 48, 799–811.e9. [PubMed: 29669253]

Suloway C, Pulokas J, Fellmann D, Cheng A, Guerra F, Quispe J, Stagg S, Potter CS, and Carragher B (2005). Automated molecular microscopy: the new Leginon system. J. Struct. Biol 151, 41–60. [PubMed: 15890530]

Tian M, Cheng C, Chen X, Duan H, Cheng H-L, Dao M, Sheng Z, Kimble M, Wang L, Lin S, et al. (2016). Induction of HIV neutralizing antibody lineages in mice with diverse precursor repertoires. Cell 166, 1471–1484.e18. [PubMed: 27610571]

Tiller T, Busse C, and Wardemann H (2009). Cloning and expression of murine Ig genes from single B cells. Journal of Immunological Methods 350, 183–193. [PubMed: 19716372]

Umotoy J, Bagaya BS, Joyce C, Schiffner T, Menis S, Saye-Francisco KL, Biddle T, Mohan S, Vollbrecht T, Kalyuzhniy O, et al.; IAVI Protocol C Investigators; IAVI African HIV Research Network (2019). Rapid and focused maturation of a VRC01-class HIV broadly neutralizing antibody lineage involves both binding and accommodation of the N276-glycan. Immunity 51, 141–154.e6. [PubMed: 31315032]

Veesler D, Cupelli K, Burger M, Gräber P, Stehle T, and Johnson JE (2014). Single-particle EM reveals plasticity of interactions between the adenovirus penton base and integrin αVβ3. Proc. Natl. Acad. Sci. USA 111, 8815–8819. [PubMed: 24889614]

Vigdorovich V, Oliver BG, Carbonetti S, Dambrauskas N, Lange MD, Yacoob C, Leahy W, Callahan J, Stamatatos L, and Sather DN (2016). Repertoire comparison of the B-cell receptor-encoding loci in humans and rhesus macaques by next-generation sequencing. Clin. Transl. Immunology 5, e93. [PubMed: 27525066]

Voss NR, Yoshioka CK, Radermacher M, Potter CS, and Carragher B (2009). DoG Picker and TiltPicker: software tools to facilitate particle selection in single particle electron microscopy. J. Struct. Biol 166, 205–213. [PubMed: 19374019]

West AP Jr., Diskin R, Nussenzweig MC, and Bjorkman PJ (2012). Structural basis for germ-line gene usage of a potent class of antibodies targeting the CD4-binding site of HIV-1 gp120. Proc. Natl. Acad. Sci. USA 109, E2083–E2090. [PubMed: 22745174]

Wickham H (2017). Tidyverse: easily install and load the “tidyverse.”. https://cran.r-project.org/web/packages/tidyverse/index.html.

Wu X, Yang Z-Y, Li Y, Hogerkorp C-M, Schief WR, Seaman MS, Zhou T, Schmidt SD, Wu L, Xu L, et al. (2010). Rational design of envelope identifies broadly neutralizing human monoclonal antibodies to HIV-1. Science 329, 856–861. [PubMed: 20616233]

Wu X, Zhou T, Zhu J, Zhang B, Georgiev I, Wang C, Chen X, Longo NS, Louder M, McKee K, et al.; NISC Comparative Sequencing Program (2011). Focused evolution of HIV-1 neutralizing antibodies revealed by structures and deep sequencing. Science 333, 1593–1602. [PubMed: 21835983]

Yacoob C, Pancera M, Vigdorovich V, Oliver BG, Glenn JA, Feng J, Sather DN, McGuire AT, and Stamatatos L (2016). Differences in allelic frequency and CDRH3 region limit the engagement of HIV Env immunogens by putative VRC01 neutralizing antibody precursors. Cell Rep. 17, 1560–1570. [PubMed: 27806295]

Zhou T, Georgiev I, Wu X, Yang Z-Y, Dai K, Finzi A, Kwon YD, Scheid JF, Shi W, Xu L, et al. (2010). Structural basis for broad and potent neutralization of HIV-1 by antibody VRC01. Science 329, 811–817. [PubMed: 20616231]

Zhou T, Zhu J, Wu X, Moquin S, Zhang B, Acharya P, Georgiev IS, Altae-Tran HR, Chuang G-Y, Joyce MG, et al.; NISC Comparative Sequencing Program (2013). Multidonor analysis reveals structural elements, genetic determinants, and maturation pathway for HIV-1 neutralization by VRC01-class antibodies. Immunity 39, 245–258. [PubMed: 23911655]

Zhou T, Lynch RM, Chen L, Acharya P, Wu X, Doria-Rose NA, Joyce MG, Lingwood D, Soto C, Bailer RT, et al.; NISC Comparative Sequencing Program (2015). Structural repertoire of HIV-1-neutralizing antibodies targeting the CD4 supersite in 14 donors. Cell 161, 1280–1292. [PubMed: 26004070]

Zivanov J, Nakane T, Forsberg BO, Kimanius D, Hagen WJ, Lindahl E, and Scheres SH (2018). New tools for automated high-resolution cryo-EM structure determination in RELION-3. eLife 7, e42166. [PubMed: 30412051]

Highlights

- The germline-targeting 426c Core immunogen elicits cross-reactive VRC01-like Abs
- Boosting with HxB2 WT Core improves the neutralizing potential of VRC01-like Abs
- Vaccine-elicited VRC01-like Abs accommodate the loop D N276-associated glycans

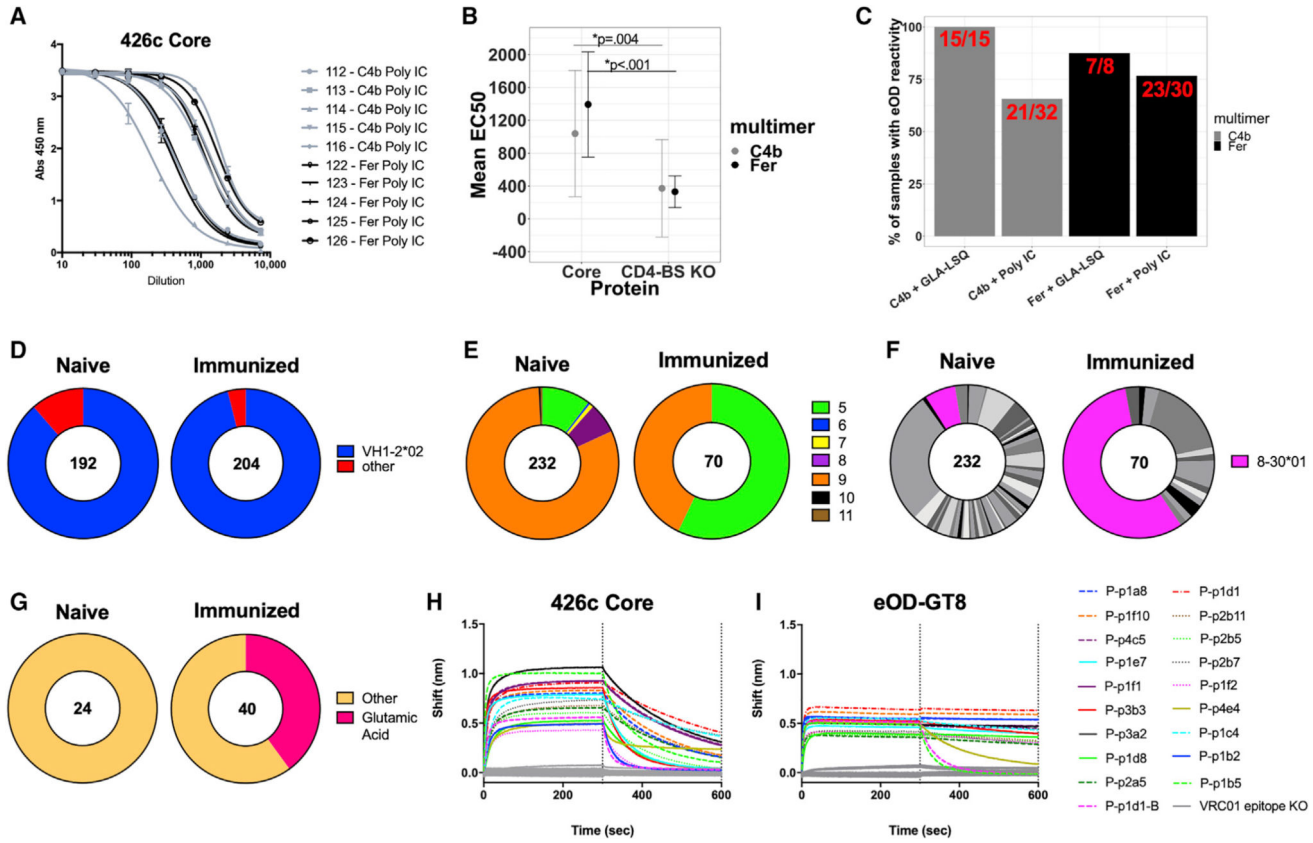

Figure 1. 426c Core Elicited Antibody and B Cell Response

(A and B) Plasma from representative animals immunized with 426c Core C4b (gray) or 426c Core Fer (black) were tested for binding against (A) 426c Core and its (B) CD4-BS KO form.

(B) Summarizes the data from one experiment with 10 animals in each group. A paired t test was used to determine statistical significance between the mean EC_{50} titers against the 426c Core versus those against its CD4-BS KO.

(C) Summary of the animal frequencies per group of 426c Core-immunized animals that developed anti-eOD-GT8 plasma antibody responses (OD 450 nm of ≥ 0.1 at 1:10 dilution; additional information is provided in Figure S1). The nanoparticle form and the adjuvant used is indicated. The number of animals that developed anti-eOD-GT8 responses out of the total immunized for each group is indicated within each bar.

(A–C) At least two biological replicates were performed for each immunization group (multimer + adjuvant).

(D–G) Pie charts indicate HC and LC sequences from individually sorted B cells from immunized (3 independent experiments) and non-immunized animals (1 experiment). The number of sequences analyzed is shown in the middle of each pie chart.

(D) HC sequences from naive and immunized animals.

(E) aa length of the CDRL3 domains in the sequences from the naive and immunized animals. 5-aa-long CDRL3s are shown in green.

(F) V-gene usage of the LCs from the sequences isolated from naive and immunized animals. The 8–30*01 V-gene is shown in pink.

(G) Presence or absence of $Glu96_{LC}$ within the LC sequences with 5-aa-long CDRL3 domains. mAbs with VRC01 characteristics were generated from paired VH/VL sequences from class-switched B cells isolated following the prime immunization (indicate by “P”) with the 426c Core.

(H) mAb binding to monomeric 426c Core (colored lines) and to monomeric 426c Core CD4-BS KO (gray lines).

(I) mAb binding to monomeric eOD-GT8 (colored lines) and to monomeric eOD-GT8 KO (gray lines). Data are representative of 1–2 experiments.

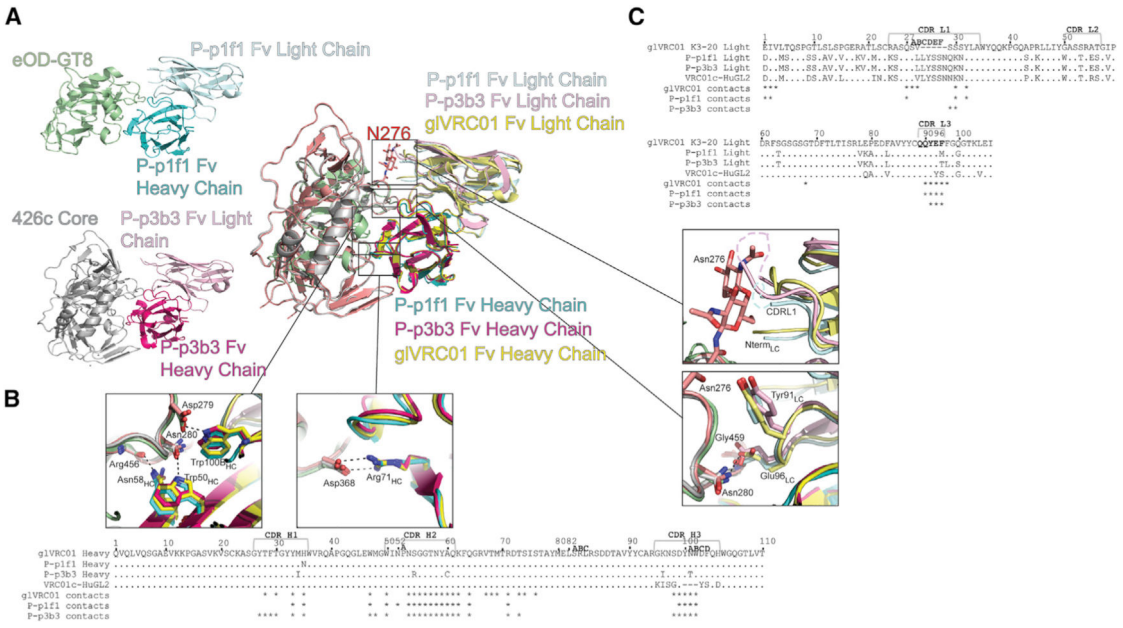

Figure 2. Structural Information of VRC01-like Antibodies Isolated after Immunization with the 426c Core Env

(A) Structures of P-p1f1 (shades of blue) in complex with eOD-GT8 (green) and P-p3b3 (shades of pink) in complex with 426c Core (gray) are shown in cartoon representation (left). These two structures are superimposed onto the structure of glVRC01 (shades of yellow) bound to 426c WT Core (orange) (PDB: 6MFT) (right). The structures are shown in ribbon representation and only the Fv portion of the Fab is shown for clarity. The glycan present at N276 in the structure of 426c WT Core bound to glVRC01 is shown in stick.

(B) Zoom insets of important contact residues in the HC of glVRC01 and VRC01-like mouse antibodies. HC sequence alignments of glVRC01, P-p1f1, P-p3b3,and VRC01c-HuGL2. Residues within 5 Å of each respective antigen are shown with an asterisk under the alignment.

(C) LC sequence alignments of glVRC01 (k3–20), P-p1f1, P-p3b3, and VRC01c-HuGL2. Residues within 5 Å of each respective antigen are shown with an asterisk under the alignment. Zoom insets of the LC N terminus, CDRL1 and CDRL3 contacts. The glycan at N276 present in the structure of glVRC01 bound to 426c WT Core is shown in sticks (PDB: 6MFT). Disordered CDRL1s are drawn in dotted lines.

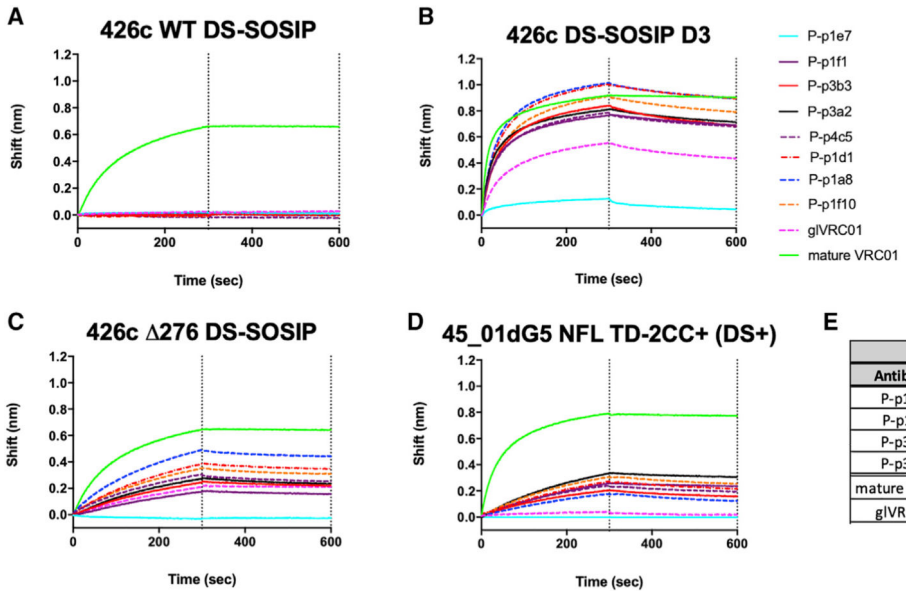

E

	WT 426c		426c △276	
Antibody	293T	GnTI-/-	293T	GnTI-/-
P-p1e7	>50	>50	>50	>50
P-p1f1	>50	>50	>50	**2.98**
P-p3b3	>50	>50	>50	**1.62**
P-p3a2	>50	>50	>50	**3.46**
mature VRC01	**2.19**	**0.11**	**0.10**	**<0.002**
glVRC01	*nt*	>100	*nt*	*nt*

Figure 3. Trimeric Env-Binding and Neutralizing Properties of VRC01-like Antibodies Elicited by the 426c Core Germline-Targeting Immunogen

(A–D) The binding of eight VRC01-like antibodies generated following the prime immunization against (A) the autologous 426c WT DS-SOSIP; (B) its variant that lacks the N276, N460, and N463 NLGS (426c DS-SOSIP D3); (C) a variant that only lacks the N276 glycan (426c Δ276 DS-SOSIP); and (D) the heterologous 45_01dG5 NFL TD-2CC+(DS+), which also lacks the N276 NLGS, was measured using Biolayer interferometry. Data are representative of 1–2 experiments.

(E) EC_{50} neutralizing titers (μg/ml) of four mAbs tested against the autologous WT 426c virus and its variant lacking the 276 NLGS, grown in either 293T cells or in 293S GnTI$^{-/-}$ cells. Mature VRC01 and glVRC01 mAbs were used as controls during these experiments. nt, not tested.

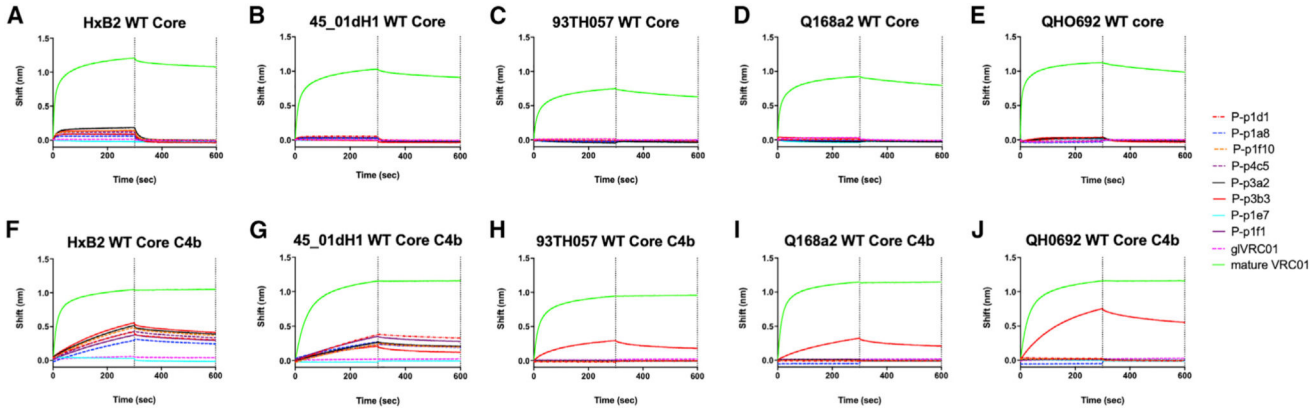

Figure 4. VRC01-like Antibodies Elicited by the 426c Core Germline-Targeting Immunogen Recognize Heterologous Wild-Type Core Env Proteins

(A–J) Biolayer interferometry binding traces of the indicated mAbs to the indicated Env proteins in either monomeric (A–E) or nanoparticle (C4b based) (F–J) forms (data are representative of 2 technical replicates). Mature and germline VRC01 mAbs were used as controls.

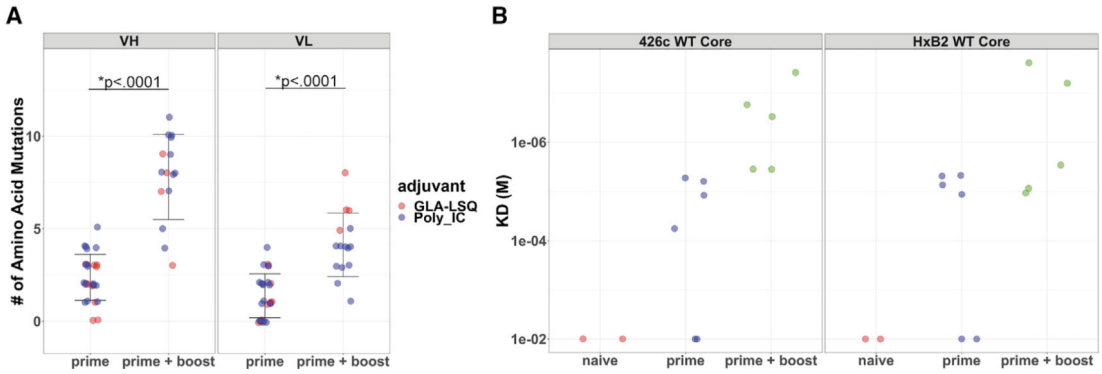

Figure 5.

VH/VL Mutations and Binding Affinities of VRC01-like Antibodies Isolated throughout the Immunization

(A) The number of aa mutations per each VH and VL domains in mAbs generated from sequences isolated following the prime immunization with 426c Core and the boost immunization with HxB2 WT Core are shown (see Figure S4 for VH and VL sequence alignments). Each dot represents a sequence. A Welch two-sample t test (unpaired t test) was used to determine the statistical significance. Error bars show SD from the mean.

(B) The binding affinities of antibodies (Fabs) isolated from naive, non-immunized animals (red) and antibodies generated after the prime immunization (blue) and following the boost immunization (green) are shown for the 426c WT Core and the HxB2 WT Core (binding traces and summary affinity information are shown in Figure S7).

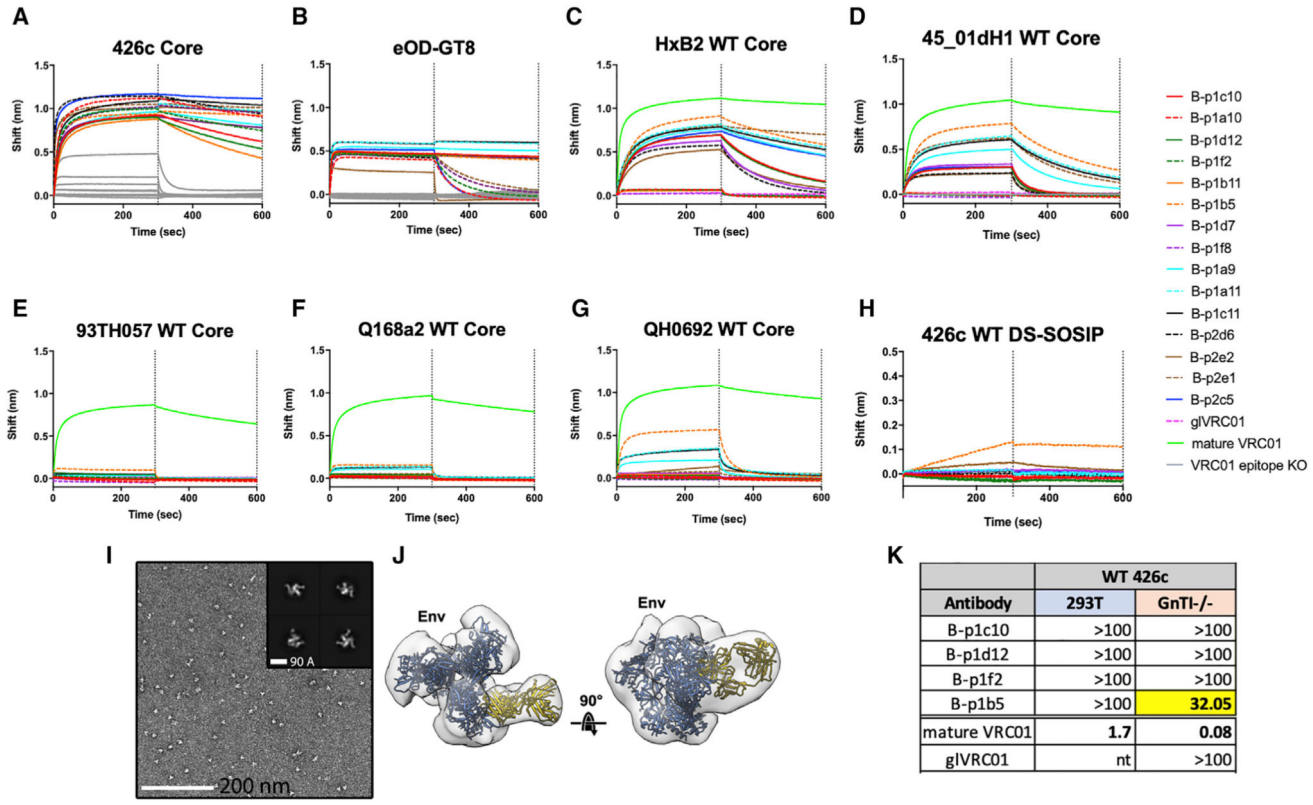

K

	WT 426c	
Antibody	293T	GnTI-/-
B-p1c10	>100	>100
B-p1d12	>100	>100
B-p1f2	>100	>100
B-p1b5	>100	**32.05**
mature VRC01	**1.7**	**0.08**
gVRC01	nt	>100

Figure 6. Env-Recognition and Neutralizing Properties of VRC01-like Antibodies Isolated following the Boost Immunization with the HxB2 WT Core Env

(A–H) Biolayer interferometry binding traces of the indicated VRC01-like mAbs isolated after the boost immunization (prefix: B) to the monomeric Env Core proteins: 426c Core (A), HxB2 WT Core (C), 45_01dH1 WT Core (D), 93TH057 WT Core (E), Q168a2 WT Core (F), QH0692 WT Core (G); monomeric eOD-GT8 (B); and the 426c WT DS-SOSIP trimeric Env (H). Mature VRC01 (green) and germline VRC01 (dashed pink) were used as controls.

(I) ns EM analysis of the 426c WT DS-SOSIP/B-p1b5 complex. Raw micrographs (scale bar, 200 nm) and 2D class averages (scale bar, 90 Å) of B-p1b5 bound to 426c WT DS-SOSIP trimers following a mild glutaraldehyde cross-linking (0.25% GTA for 45 s followed by quenching with 1 M Tris) to increase saturation of the 426c WT DS-SOSIP trimer.

(J) 3D reconstruction of the negatively stained 426c WT DS-SOSIP/B-p1b5 complex cross-linked with 0.25% GTA. Structures of the 426c DS-SOSIP D3 trimer and germline VRC01 Fab were fit to the density as a reference (gray, ns EM density; blue, 426c DS-SOSIP D3; yellow, Fab) (Borst et al., 2018).

(K) EC_{50} neutralizing titers (in micrograms per milliliter) of indicated mAbs against the WT 426c virus grown in either 293T cells of 293S GnTI$^{-/-}$ cells. Mature and germline VRC01 mAbs were used as controls for the binding and neutralization assays. Neutralization assays against the GnTI$^{-/-}$ produced virus were performed 2–3 times. Neutralization assays against the 293T produced virus is from one experiment. nt, not tested.

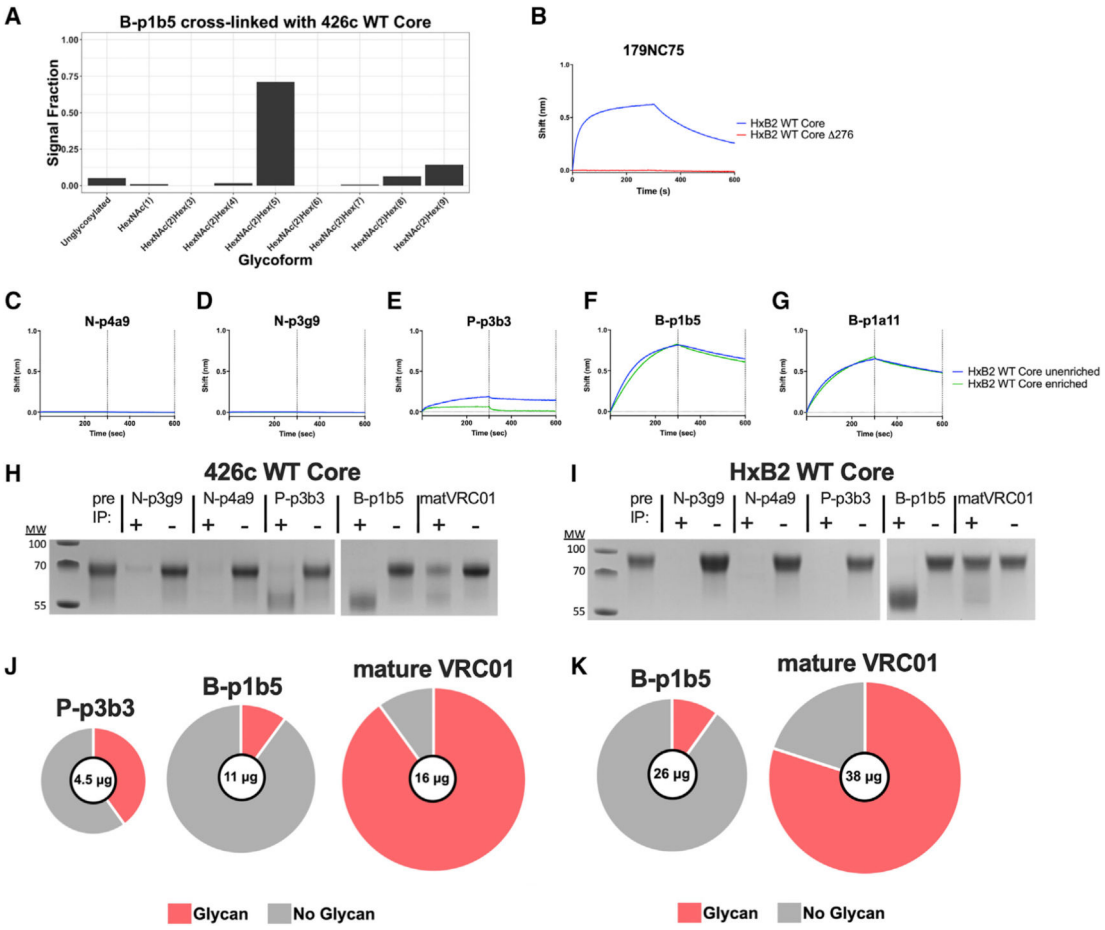

Figure 7. Vaccine Elicited Antibodies Bind in to Env Core with Glycans at N276

(A) The 426c WT Core/B-p1b5 complex was generated in 293 GnTI$^{-/-}$ cells, purified, and subjected to semiquantitative LC-MS/MS analysis. Depicted here are the relative signal intensities of (glyco)peptides comprising the 276 NLGS. The mass spectrometry data represent the average of two technical replicates.

(B) Binding of mAb 179NC75 to HxB2 WT Core or its derivative lacking the N276 NLGS ("HxB2 WT Core Δ276"). Data are representative of two technical replicates.

(C–G) Binding of the mAbs N-p4a9 (C), N-p3g9 (D), P-p3b3 (E), B-p1b5 (F), and B-p1a11(G) to HxB2 WT Core that has been enriched for the glycan at 276 (eluted from a 179NC75 column) or the unenriched fraction.

(H and I) mAbs generated from unimmunized animals (N-p3g9 and N-p4a9), from animals immunized with the 426c Core (P-p3b3), and from animals immunized with the 426c Core and the HxB2 WT Core (B-p1b5) were immobilized on beads. The beads were incubated with 426c WT Core or HxB2 WT Core proteins expressed in 293 GnTI$^{-/-}$ cells. Following co-immunoprecipitation, 426c WT Core (H) and HxB2 WT Core (I) were washed and eluted from the beads. (H and I) A fraction of the unbound ("−") and the eluted ("+") material was subjected to SDS-PAGE gel electrophoresis. The gel is representative of two technical replicates. (J and K) The eluted fractions were further subjected to semiquantitative LC-MS/MS analysis (two technical replicates) to determine the presence of a glycan at position 276 on 426c WT Core (J) and on HxB2 WT Core (K). The quantity of material eluted from

the beads after co-immunoprecipitation is shown in the middle of the pie charts, which are scaled relative to the amount of material pulled down with mature VRC01.

KEY RESOURCES TABLE

REAGENT or RESOURCE	SOURCE	IDENTIFIER
Antibodies		
FITC Rat Anti-Mouse IgG1 (clone A85–1)	BD Biosciences	Cat# 553443; RRID:AB_394862
FITC Rat Anti-Mouse IgG2b (clone R12–3)	BD Biosciences	Cat# 553395; RRID:AB_394833
Goat anti Mouse IgG2c:FITC	Bio-Rad	Cat# STAR135F; RRID:AB_1102667
FITC Rat Anti-Mouse IgG3 (clone R40–82)	BD Biosciences	Cat# 553403; RRID:AB_394840
PerCP/Cy5.5 anti-mouse IgD Antibody	Biolegend	Cat# 405710; RRID:AB_1575113
Anti-Human/Mouse GL7 eFluor 450	Thermo Fisher Scientific	Cat# 48–5902–80; RRID:AB_10854881
eBioscience Fixable Viability Dye eFluor 506	Thermo Fisher Scientific	65–0866–14
BV510 Hamster Anti-Mouse CD3e (clone 145–2c11)	BD Biosciences	Cat# 563024; RRID:AB_2737959
BV510 Rat Anti-Mouse CD4 (clone RM4–5)	BD Biosciences	Cat# 563106; RRID:AB_2687550
BV 510 Rat Anti-Mouse Ly-6G and Ly6C (clone RB6–8C5)	BD Biosciences	Cat# 563040; RRID:AB_2722496
Brilliant Violent 510 anti-mouse F4/80 Antibody	Biolegend	Cat# 123135; RRID:AB_2562622
Brilliant Violet 605 anti-mouse IgM Antibody	Biolegend	Cat# 406523; RRID:AB_2563358
BV786 Rat Anti-Mouse CD45R/B220	BD Biosciences	Cat# 563894; RRID:AB_2738472
Anti-Mouse CD38 Alexa Fluor 700	Thermo Fisher Scientific	Cat# 56–0381–82; RRID:AB_657740
BUV395 Rat Anti-Mouse CD19 (clone 1D3)	BD Biosciences	Cat# 563557; RRID:AB_2722495
BV650 Rat Anti-Mouse CD19	BD Biosciences	Cat# 563235; RRID:AB_2738085
6x-His Tag Monoclonal Antibody (HIS.H8)	Thermo Fisher Scientific	Cat# MA1–21315; RRID:AB_557403
HRP Goat anti-mouse IgG	Biolegend	Cat# 405306; RRID:AB_315009
Bacterial and Virus Strains		
NEB® 5-alpha Competent *E. coli* (High Efficiency)	New England BioLabs	C2987H
HIV-1 Env-pseudotyped viruses	D. Montefiori and C. LaBranche, Duke University	N/A
Chemicals, Peptides, and Recombinant Proteins		
Poly(I:C)	Invivogen	tlrl-pic-5
GLA-LSQ	Infectious Disease Reseach Institute (IDRI)	IDRI-LS130
Steptavidin-R-Phycoerythirin	Prozyme	PJRS25
Streptavidin-Allophycocyanin	Prozyme	PJ27S
RNaseOUT Recombinant Ribonuclease Inhibitor	Thermo Fisher Scientific	10777019
HotStar Taq Plus	QIAGEN	203607
Gel Red Nucleic Acid Stain	Biotium	41002
ExoSap-IT	Affymetrix	78201
Endoproteinase LysC	New England BioLabs	P8109S
Endo H	New England BioLabs	P0702S
Uranyl Formate	Electron Microscopy Sciences	22451

REAGENT or RESOURCE	SOURCE	IDENTIFIER
SureBlue Reserve TMB Microwell Peroxidase Substrate	KPL	53–00–02
293-Free Transfection Reagent	Millipore Sigma	72181
5x In-Fusion enzyme	Takara Bio	1805251A
Pierce Trypsin Protease	Thermo Fisher Scientific	90057
SuperScript IV RT	Thermo Fisher Scientific	18090200
Accuprime Pfx Supermix	Thermo Fisher Scientific	1244040
Critical Commercial Assays		
EasySep Mouse B Cell Isolation Kit	StemCell Technologies, Inc.	19854
InFusion HD Cloning Kit	Takara Bio	639649
QIAprep Spin Miniprep Kit	QIAGEN	27106
britelite plus Reporter Gene Assay System	PerkinElmer	6066766
Thrombin, Restriction Grade	EMD Millipore	69671–3
Deposited Data		
P-p3b3Fab + 426c Core structure	This paper	Protein Data Bank, PDB ID: 6MFT
P-p1f1Fab + eOD-GT8 structure	This paper	Protein Data Bank, PDB ID: 4JPK
Mass Spectrometry Data	This paper	PRIDE: PXD015168
Sequence analysis code	This paper	GitHub, https://github.com/krparks/glVRC01_sequential_immunization
Antibody and protein sequences	This paper	GenBank, Table S5
Experimental Models: Organisms/Strains		
Mouse: glH-VRC01	Jardine et al., 2015	N/A
Oligonucleotides		
Random Primers	Thermo Fisher Scientific	48190011
GeneAmp dNTP Blend	Thermo Fisher Scientific	N8080261
Primers for PCR	This paper; Jardine et al., 2015; Tiller et al., 2009	Table S3
Recombinant DNA		
Ptt3 k vector	Snijder et al., 2018	N/A
PMN 4–341 vector	Mouquet et al., 2010	N/A
Software and Algorithms		
Geneious (Version 8.1.9)	Biomatters Ltd.	https://www.geneious.com
R (Version 3.4.1)	R Core Team, 2018	https://www.R-project.org/
IMGT/V-QUEST	Brochet et al., 2008; Giudicelli et al., 2011	http://www.imgt.org/IMGT_vquest/input
Tidyverse	Wickham, 2017	https://cran.r-project.org/web/packages/tidyverse/index.html
Biostrings	Pages et al., 2018	http://bioconductor.org/packages/release/bioc/html/Biostrings.html
Prism 7	GraphPad	https://www.graphpad.com
seqinr	Charif and Lobry, 2007	N/A
Other		

REAGENT or RESOURCE	SOURCE	IDENTIFIER
Anti-PE microbeads	Miltenyi Biotech	130–048–801
Anti-APC microbeads	Miltenyi Biotech	130–090–855
LS Columns	Miltenyi Biotech	130–042–401
Pierce Protein A agarose beads	Thermo Fisher Scientific	20334
Anti-human IgG Fc Capture (AHC) Biosensors	ForteBio	18–5063
Anti-Human Fab-CH1 2nd Generation (FAB2G) Biosensors	ForteBio	18–5126
MyOne Tosylactivated Dynabeads	Thermo Fisher Scientific	65501
His60 Ni-Superflow Resin	Takara Bio	636660
HiLoad 16/600 Superdex 200 pg (GE) column	GE Healthcare	28989335
Superose 6 10/300 GL	GE Healthcare	17–6172–01
Agarose Bound Galanthus Nivalis Lectin	Vector Labs	AL-1243–5
Step-Tactin SuperFlow Plus	QIAGEN	30002
HisTrap FF Column	GE Healthcare	17525501